

# The stellar IMF in early-type galaxies from a non-degenerate set of optical line indices.

Chiara Spiniello<sup>1,2\*</sup>, Scott Trager<sup>1</sup>, Léon V.E. Koopmans<sup>1</sup>, Charlie Conroy<sup>2</sup>

<sup>1</sup>*Kapteyn Astronomical Institute, University of Groningen, PO Box 800,9700 AV Groningen, the Netherlands*

<sup>2</sup>*Now at: Max-Planck Institute for Astrophysics, Karl-Schwarzschild-Strasse 1, 85740 Garching, Germany*

<sup>3</sup>*Department of Astronomy & Astrophysics, University of California, Santa Cruz, CA, USA*

Accepted Year Month Day. Received Year Month Day; in original form Year Month Day

## ABSTRACT

We investigate the optical spectral region of spectra of  $\sim 1000$  stars searching for IMF-sensitive features to constrain the low-mass end of the initial mass function (IMF) slope in elliptical galaxies. The use of indicators bluer than NIR features (NaI, CaT, Wing-Ford FeH) is crucial if we want to compare our observations to optical simple stellar population (SSP) models. We use the MILES stellar library (Sánchez-Blázquez et al. 2006) in the wavelength range 3500–7500 Å to select indices that are sensitive to cool dwarf stars and that do not or only weakly depend on age and metallicity. We find several promising indices of molecular TiO and CaH lines. In this wavelength range, the response of a change in the effective temperature of the cool red giant (RGB) population is similar to the response of a change in the number of dwarf stars in the galaxy. We therefore investigate the degeneracy between IMF variation and  $\Delta T_{\text{eff,RGB}}$  and show that it is possible to break this degeneracy with the new IMF indicators defined here. In particular, we define a CaH1 index around  $\lambda 6380$  Å that arises purely from cool dwarfs, does not strongly depend on age and is anti-correlated with  $[\alpha/\text{Fe}]$ . This index allows the determination of the low-mass end of the IMF slope from integrated-light measurements when combined with different TiO lines and age- and metallicity-dependent features such as H $\beta$ , Mgb, Fe5270 and Fe5335. The use of several indicators is crucial to break degeneracies between IMF variations, age, abundance pattern and effective temperature of the cool red giant (RGB) population. We measure line-index strengths of our new optical IMF indicators in the Conroy & van Dokkum (2012a) SSP models and compare these with index strengths of the same spectral features in a sample of stacked Sloan Digital Sky Survey (SDSS) early-type galaxy (ETG) spectra with varying velocity dispersions. Using different indicators, we find a clear trend of a steepening IMF with increasing velocity dispersion from 150 to 310 km s<sup>-1</sup> described by the linear equation  $x = (2.3 \pm 0.1) \log \sigma_{200} + (2.13 \pm 0.15)$ , where  $x$  is the IMF slope and  $\sigma_{200}$  is the central stellar velocity dispersion measured in units of 200 km s<sup>-1</sup>. We test the robustness of this relation by repeating the analysis with ten different sets of indicators. We found that the NaD feature has the largest impact on the IMF slope, if we assume solar  $[\text{Na}/\text{Fe}]$  abundance. By including NaD the slope of the linear relation increases by 0.3 ( $2.6 \pm 0.2$ ). We compute the “IMF mismatch” parameter as the ratio of stellar mass-to-light ratio predicted from the  $x - \sigma_{200}$  relation to that inferred from SSP models assuming a Salpeter IMF and find good agreement with independent published results.

**Key words:** dark matter — galaxies: elliptical and lenticular, cD — gravitational lensing: strong — galaxies: kinematics and dynamics — galaxies: evolution — galaxies: structure

## 1 INTRODUCTION

The stellar contribution to the mass budgets of early-type galaxies (ETGs) is a crucial ingredient to fully understand

\* E-mail: spiniello@astro.rug.nl

the internal structure, the formation and the evolution of these massive galaxies (e.g. Blumenthal et al. 1984). In ETGs the stellar mass-to-light ratio ( $\Upsilon_*$ ) scales with the luminous mass of the system (Grillo et al. 2009; Barnabè et al. 2011; Dutton, Mendel & Simard 2012; Cappellari et al. 2012; Tortora, Romanowsky & Napolitano 2013), but it has also been shown recently that, for the assumption of a universal initial mass function (IMF), the dark matter (DM) fraction in the internal region of these systems increases with the mass of the galaxy (e.g. Zaritsky, Gonzalez & Zabludoff 2006; Auger et al. 2010a; Treu et al. 2010; Barnabè et al. 2011). Disentangling the relative contributions of baryonic and dark matter constituents of ETGs is therefore crucial to fully comprehend the processes that shape the hierarchical galaxy formation scenario (e.g. White & Rees 1978; Davis et al. 1985; Frenk et al. 1985).

A quantitative study of the luminous unresolved stellar content of distant galaxies requires the use of stellar population synthesis models (Worthey 1994; Renzini 2006; Conroy 2013). By comparing colors, line-strength indices or full spectral energy distributions (SEDs) in galaxy spectra with predictions from single stellar population (SSP) models (which assume a single epoch of star formation rather than an extended SFH), it is possible to derive stellar parameters such as luminosity-weighted age, metallicity,  $\Upsilon_*$ , IMF slope and elemental abundances for a galaxy (Worthey 1994; Trager et al. 2000a,b). However, it remains difficult to trace a galaxy’s full star formation history (SFH), to break the age-metallicity degeneracy (Worthey 1994) and to study possible correlation of IMF slope and  $\alpha$ -enhancement variation with galaxy masses (Spinrad 1962; Spinrad & Taylor 1971; Cohen 1978; Frogel et al. 1978; Frogel, Persson & Cohen 1980; Faber & French 1980; Carter, Visvanathan & Pickles 1986; Hardy & Couture 1988; Couture & Hardy 1993; Worthey 1994; Cenarro et al. 2003).

In the last two decades a crucial assumption has been made in constraining the star formation history of galaxies through SSPs: the IMF is assumed to be universal and equal to that of our Milky Way (Kroupa 2001; Chabrier 2003; Bastian, Covey & Meyer 2010). In the past years, evidence has emerged that the IMF might evolve (Davé 2008; van Dokkum 2008) and may depend on the (stellar) mass of the system (e.g. Treu et al. 2010; Auger et al. 2010b; Napolitano, Romanowsky & Tortora 2010; van Dokkum & Conroy 2010; Spiniello et al. 2011, 2012). Recently, van Dokkum & Conroy (2010), hereafter vDC10, have suggested that low-mass stars ( $\leq 0.3 M_\odot$ ) could be much more prevalent in massive early-type galaxies (ETGs) than previously thought. This could imply that the increase in the  $\Upsilon_*$  with galaxy mass is due to a steeper low-mass end of the IMF rather than an increasing fraction of internal DM (Treu et al. 2010; Auger et al. 2010a; Barnabè et al. 2011; Dutton, Mendel & Simard 2012; Cappellari et al. 2012; Spiniello et al. 2012).

Strong absorption features that vary with surface gravity at fixed effective temperature and that can be used to count stars with masses  $\leq 0.3 M_\odot$  (M dwarfs) are mainly present in the red-optical and near-infrared spectral region (vDC10, Smith, Lucey & Carter 2012). At these wavelengths galaxy stellar emission is dominated by evolved stellar populations, i.e. red giant branch (RGB) and asymptotic giant branch (AGB) stars (e.g. Worthey 1994; Renzini 2006), whose physics is not yet well understood, because their life-

time is very short and mass-losses are very high (e.g. Reimers 1975). Moreover, AGB stars are also highly variable (e.g. Blöcker 1995). In the optical spectral region, on the other hand, M dwarfs contribute at most 5% to the total light of the integrated spectrum, despite dominating the total stellar mass budget in galaxies (Worthey 1994). The light in ETGs is dominated by K and M giants, that, to the first order, have spectra similar to the one of an M dwarf, because of the similar spectral type. However the spectra of M dwarfs and M giants with similar effective temperature show minor but important differences. Careful line-index strength measurements of multiple spectral indices (or full spectral fitting: Conroy & van Dokkum 2012b) are necessary to reveal these spectral differences at the percent level and to break degeneracies, enabling one to observe variations of IMF with galaxy mass if present.

Two new SSP models have recently been published specifically for the purpose of measuring the IMF slope down to  $\sim 0.1 M_\odot$  for old, metal-rich stellar populations. Conroy & van Dokkum (2012a), hereafter CvD12, built models over the wavelength interval  $0.35 \mu\text{m} < \lambda < 2.4 \mu\text{m}$  at a resolving power of  $R \sim 2000$ , using a combination of two empirical stellar libraries (MILES, Sánchez-Blázquez et al. 2006; and IRTF, Cushing, Rayner & Vacca 2005) and three sets of isochrones. Vazdekis et al. (2012) recently built the MIUSCAT models, an extension in wavelength of the Vazdekis et al. (2003a,b, 2010) models.

All other available models in the NIR are based on theoretical atmospheres and stellar libraries (Maraston 2005; Bruzual & Charlot 2003), which have only been tested by fitting broadband colors and do not reproduce line indices measurements of clusters and galaxies (Lyubenova et al. 2012). The CvD12 and MIUSCAT models are therefore the state-of-the-art of SSP models.

Both models allow for different IMF slopes and a range of ages, but while the CvD12 models use solar metallicity isochrones and synthesize models with different abundance patterns, MIUSCAT models use different total metallicities but do not allow one to change the abundances which are fixed to solar. Non-solar abundance patterns appear to be a necessary ingredient to properly assess the non-universality of the IMF, especially in massive ETGs, which may have undergone a star formation histories different from the solar-neighbourhood (Peterson 1976; Peletier 1989; Worthey 1992; Trager et al. 2000b; Arrigoni et al. 2010). The CvD12 models allow for a variation in  $[\alpha/\text{Fe}]$  as well as the abundance pattern of 11 different elements. This is particularly important in the case of sodium lines, especially when including the NaD index. As shown in Conroy & van Dokkum (2012a,b) and confirmed in Spiniello et al. (2012), more massive systems seem to be Na-enhanced ( $[\text{Na}/\text{Fe}] \sim 0.3\text{--}0.4$  dex), consistent with values obtained for the bulge of the Milky Way (on average  $[\text{Na}/\text{Fe}] \sim 0.2$ , Fulbright, McWilliam & Rich 2007); see Spiniello et al., in prep., for a detailed study of the impact of models with and without variable abundance patterns on the determination of the low-mass IMF slope in ETGs. We therefore use the CvD12 models in this study to have the required ability to decouple IMF variations from abundance variations. Moreover, CvD12 also include the possibility to change the effective temperature of the red giant branch (RGB), taking into account that the isochrones should change with abundance pattern.

In the blue region (3500–7500 Å) the CvD12 and MIUSCAT models use the same empirical spectral library (MILES), while in the red and NIR they make use of two different libraries (CvD12 uses IRTF, MIUSCAT uses Indo-US, Valdes et al. 2004, and CaT, Cenarro et al. 2001). The use of optical indicators allows us to reduce the uncertainties caused by different assumptions of different SSP models in the synthesis process (e.g. their spectral libraries).

Conroy & van Dokkum (2012b) clearly show that there is information on the IMF slope in the blue spectral range, the goal of this work is to recover and quantify this information. We find a set of optical IMF-sensitive spectral indicators that allow us to decouple the effects of a varying IMF from age, metallicity and/or elemental abundance variations, and the effective temperature of the RGB, when studying the stellar populations of massive ETGs. A direct comparison of the variation of index strengths with IMF slope predicted from the SSP models with the variation of index strengths determined from SDSS spectra allows us to understand whether the recent suggestion that the IMF steepens with increasing galaxy velocity dispersion is genuine or arises from a misunderstanding of the main ingredients of SSP models.

In this work (i) we focus on line-index measurements rather than full spectral fitting, which avoids issues with spectral calibration when comparing to observations that might have been poorly calibrated and (ii) we assume an SSP, rather than an extended SFH, which is still a strong assumption and will be properly addressed in future works. The paper is organized as follows. In Section 2 we present a new set of IMF-sensitive indicators along with a brief introduction of the MILES library. In Section 3 we compare line-index variations as function of the IMF slope from single MILES stars and the CvD12 SSP model. In Section 4 we compare the models with SDSS galaxies. We summarize our findings and discuss our conclusions in Section 5.

## 2 NEW OPTICAL IMF-SENSITIVE INDICES

Stellar spectral features that show different strengths in M-dwarfs and cool giants, including NaI, Wing-Ford FeH, CaT and CaI, can potentially reveal a galaxy’s low-mass stellar content in spectra of unresolved stellar populations (e.g. Spinrad 1962; Faber & French 1980; Schiavon et al. 1997; Schiavon, Barbay & Singh 1997; Schiavon, Barbay & Bruzual A. 2000; Cenarro et al. 2003). These are mainly present in the red-optical and near-infrared part of the spectra. However, optical spectra are easier to obtain with current spectrographs than NIR (1–2  $\mu$ m) spectra. Moreover, near-infrared spectra are contaminated by the presence of strong sky lines and telluric absorption arising from water vapour (e.g. Stevenson 1994). A proper measurement of equivalent widths (EW) in the red part of the spectrum relies heavily on the correct removal of these lines. It is therefore important to search for IMF-sensitive features in the blue-optical spectral region, where the SSP models are less affected by these uncertainties and different assumptions. However one has to keep in mind that blue-optical spectral features are more sensitive to stars of earlier spectral types.

### 2.1 Searching for IMF-sensitive features in the MILES Library

We searched for spectral features that would be sensitive to IMF variations in SSPs by searching for features that appear solely in cool dwarf stars in the MILES empirical spectral stellar library (Sánchez-Blázquez et al. 2006), the same library used by the CvD12 and MIUSCAT models. The MILES library consists of  $\sim 1000$  stellar spectra obtained at the 2.5m INT telescope. It covers the wavelength range 3525–7500 Å with 2.51 Å (FWHM) spectral resolution and spans a large range in atmospheric parameters:  $[\text{Fe}/\text{H}] = [-2.86, 1.65]$ ,  $\log g = [-0.2, 5.5]$  and  $T_{\text{eff}} = [2747, 36000]$ . Using these spectra, we identified a number of potentially interesting stellar features that could be used to constrain the low-mass end of the IMF. We plotted the ratio between spectra of a cool giant ( $T_{\text{eff}} \sim 3300\text{K}$ ) and a cool dwarf ( $T_{\text{eff}} \sim 2800\text{K}$ ), both with roughly solar metallicity, to select these spectral features. We inspected this ratio looking for wavelength regions with large residuals. We identified seven interesting regions, including four new and previously unidentified features, and defined absorption-line indices for these. Moreover, we ran a principal component analysis on the SSP models to isolate features that strongly depend on temperature and gravity. The final IMF-sensitive indices we have found and use here are listed in Table 1. We note that TiO and CaH indices are measured in magnitudes, while NaD is measured in Å.

Figures 1 and 2 show index strengths of these indices for single MILES stars as a function of temperature (left panels), gravity (middle panels) and metallicity (right panels). The figures clearly show that all the selected stellar absorption features are very weak in main-sequence stars (MS) and intermediate-temperature stars and are strong in cool dwarfs and giants – except CaH1, which is only strong in cool dwarfs–.

More than half of the selected indices come from TiO molecular absorption bands (Fig. 1). The effect of TiO lines in stellar atmospheres has been extensively studied over the years (Jorgensen 1994; Allard, Hauschildt & Schwenke 2000; Valenti, Ferraro & Origlia 2010) and red TiO lines have already been recognized to be good IMF indicators (Spiniello et al. 2012, Chen et al. 2013, in prep.). Our bluest feature is around  $\lambda \sim 4770$  Å: we call it blue-TiO and define a new index (bTiO, Table 1). Although a similar index was already used in Serven, Worthey & Briley (2005), who named it Mg4780, we are confident that this absorption is due to TiO molecular lines, whose strength is very large in very cool dwarf and giant stars and smaller for intermediate-mass M stars, as shown in the middle panel of Figure 1. The aTiO index, defined around the  $\alpha$ -TiO feature (Jorgensen 1994), is also strongly IMF-sensitive. A possible issue with this feature is the presence in its central bandpass of the very strong [OI]  $\lambda 5577$  Å sky emission line. Any contamination from sky lines could affect the response to gravity of the spectral index defined around aTiO. However from Figure 1 it appears that the subtraction of the emission line in the library stars is sufficient, as the behaviour of aTiO seems to be similar to that of bTiO and TiO2 (i.e., stronger EWs for cool giants and dwarfs). The TiO2 feature ( $\lambda \sim 6230$  Å) was already found to be promising in constraining the low-mass end of the IMF slope (see Spiniello et al. 2012), but it also shows a weak de-

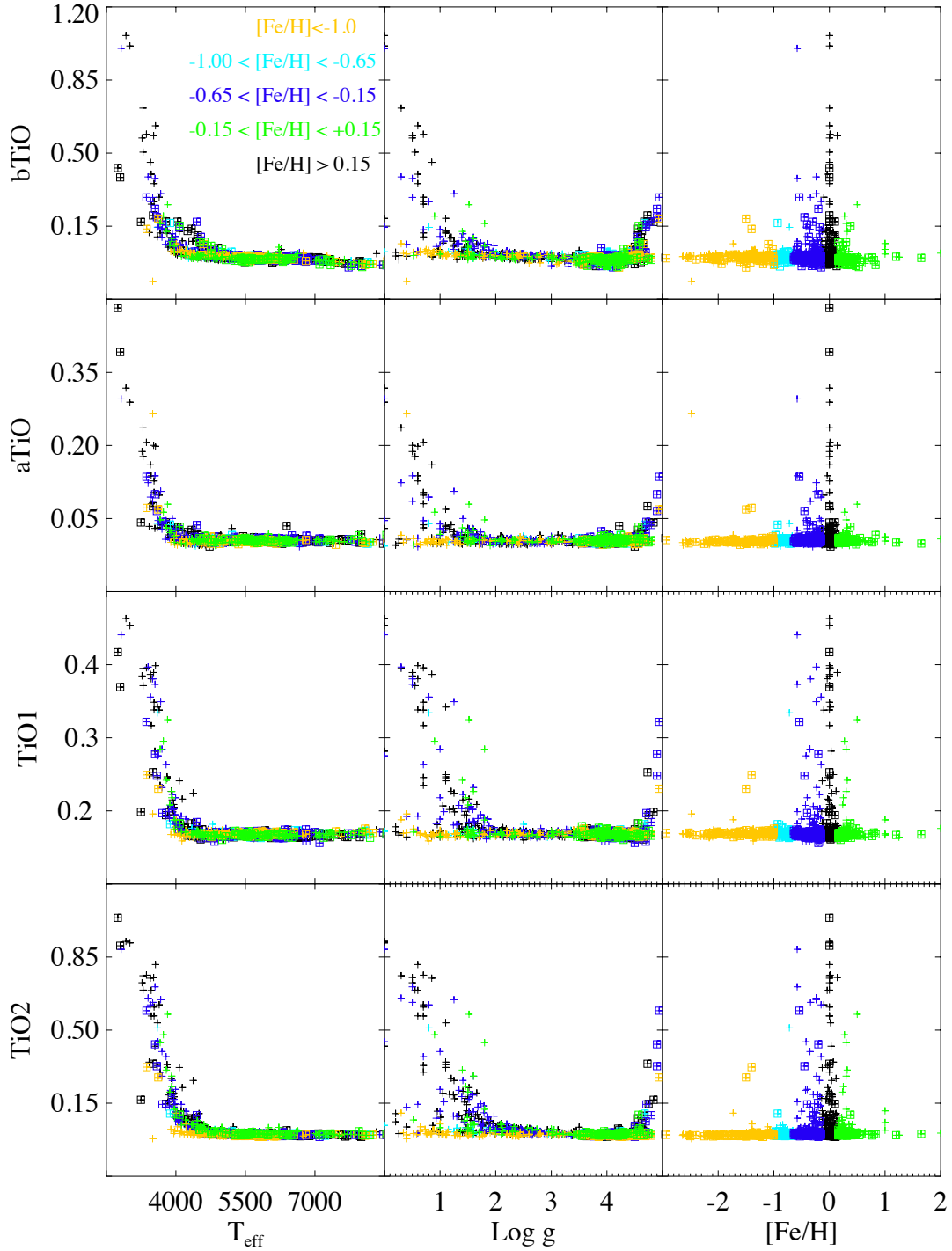


**Figure 1.** Index strengths of TiO indices for single stars from the MILES library plotted as function of temperature, gravity, and  $[\text{Fe}/\text{H}]$ , at the original MILES resolution. The points are coded by  $\log g$ : crosses are mostly giants, and squares are dwarfs. The colors refer to  $[\text{Fe}/\text{H}]$ , as seen in the upper-left panel. All TiO indices are very strong in cool stars ( $T < 4100\text{K}$ ). From the middle panel, it is clear that the indices are stronger in giants (i.e.  $\log g < 3.0$ ) and M dwarfs (i.e.  $\log g > 3.8$ ) than in warmer main-sequence stars.

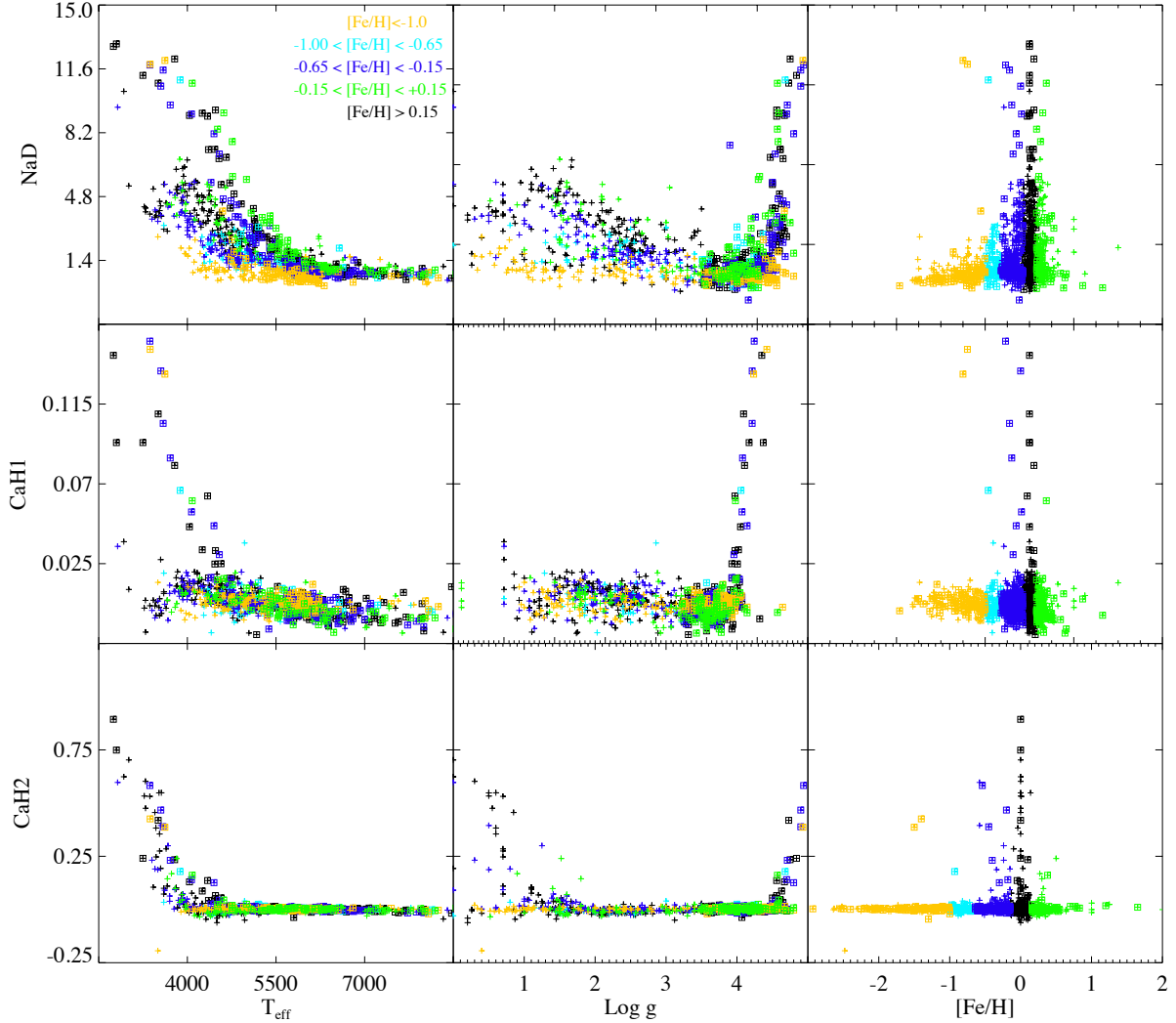


**Figure 2.** EWs of CaH and NaD indices for single stars from the MILES library plotted as function of temperature, gravity, and  $[\text{Fe}/\text{H}]$ , at the original MILES resolution. The points are coded by  $\log g$ : crosses are mostly giants, and squares are dwarfs. The colors refer to  $[\text{Fe}/\text{H}]$ , as seen in the upper-left panel. The middle row shows the only feature which is very strong only in cool stars ( $T < 4500\text{K}$ ) with high gravity (i.e.  $\log g > 3.8$ ): CaH1. This index allows us to count the M-dwarf population in a galaxy spectrum.

pendence on metallicity and  $\alpha$ -element variation (Chen et al. 2013, in prep). The NaD feature, although gravity-sensitive, also depends strongly on abundance (in particular this index is  $\sim 4$  times more sensitive to variation in the  $[\text{Na}/\text{Fe}]$  abundance than to variation of the IMF slope, as shown in Spiniello et al. (2013, in prep.) and may be contaminated by the interstellar medium (e.g. Spiniello et al. 2012).

As a sanity check, we show spectra of single dwarf stars with similar gravity ( $\log g = 4.6\text{--}5$ ) at different values of  $T_{\text{eff}}$  in the left panels of Figure 3 in order to ensure that these indices are stronger in cool dwarfs than in warm ones. The right panels of Figure 3 show instead spectra of single cool giants with a range of effective temperatures. bTiO and TiO<sub>2</sub> are clearly stronger in cool stars but they behave simi-

larly in giants and dwarfs, therefore they do not allow one to disentangle between these two classes of stars and between a top-heavy and a bottom-heavy IMF by themselves.

However, the CaH1 index around  $\lambda 6380 \text{ \AA}$  (Fig. 2), is strong only in cool dwarfs. We believe that this feature is the most robust optical feature to estimate the IMF in this particular wavelength region, because it allows us to disentangle the contribution of RGB stars from the cool M-dwarf population when combined with age- and metallicity-sensitive features. CaH features were first detected in spectra of M dwarfs by Fowler (1907) and then studied in detail by Öhman (1934). Already in that paper Öhman pointed out that the CaH band at  $6390 \text{ \AA}$  (corresponding to our CaH1 index) is strong in M-dwarf spectra and almost absent in

**Table 1.** Definition of the IMF-sensitive indices used in this paper. TiO and CaH indices are measured in magnitudes, while NaD is measured in Å

Index	Central band (Å)	Pseudo-continua (Å)
bTiO	4758.500 – 4800.000	4742.750 – 4756.500
		4827.875 – 4847.875
aTiO	5445.000 – 5600.000	5420.000 – 5442.000
		5630.000 – 5655.000
NaD	5876.875 – 5909.375	5860.625 – 5875.625
		5922.125 – 5948.125
TiO1	5936.625 – 5994.125	5816.625 – 5875.625
		6038.625 – 6103.625
TiO2	6189.625 – 6272.125	6066.625 – 6141.625
		6372.625 – 6415.125
CaH1	6357.500 – 6401.750	6342.125 – 6356.500
		6408.500 – 6429.750
CaH2	6775.000 – 6900.000	6510.000 – 6539.250
		7017.000 – 7064.000

M giants. Mould (1976) realized that the behaviour of CaH in stellar atmospheres is strongly influenced by gas pressure over the formation of the molecule, and therefore he used the CaH band as a luminosity indicator of cool stars in low resolution spectra. He also studied the sensitivity of the CaH band strength to gravity, clearly confirming that CaH bands are very weak or absent in giants. Finally, Barbuy et al. (1993) presented a study of the intensity of CaH bands as a function of stellar temperature and gravity. Their results are qualitatively consistent with ours in the sense that CaH absorption lines are stronger in dwarfs and tend to disappear in giants. We refer to section 5.4 of Conroy & van Dokkum (2012a) for a useful sketch of the basic physics involved.

This brief historical overview demonstrates that it has been known for a hundred years that certain spectral features depend strongly on surface gravity at fixed effective temperature and therefore betray the presence of faint M dwarfs in integrated light spectra.

From Figure 3, it is clear that the spectrum of a cool giant is similar to that of a cool dwarf. We therefore also investigate the response of variation in the effective temperature of red-giant branch versus the response in variation of the IMF slope, to ensure that the degeneracy between  $T_{\text{eff,RGB}}$  and IMF slope can be broken by our optical IMF indicators. Indeed, one of the problems that one faces when using indices bluer than  $\sim 7500$  Å is that the effects of a varying IMF and of a varying  $T_{\text{eff}}$  of the isochrones are very similar, as shown in Figure 4.

In the figure we plot the continuum normalized response to IMF variation and variation of the value of  $T_{\text{eff}}$  of the RGBs as a function of wavelength. As expected, the IMF variation is *almost* completely overwhelmed by  $T_{\text{eff}}$  variation. However, the two curves differ in their responses around bTiO, aTiO and CaH1. Therefore only the use of the full set of lines allows one to separate IMF and  $T_{\text{eff}}$  effects. By combining blue spectral features that strongly depend on age, metallicity and elemental abundance with surface-gravity-sensitive features, such as TiO and CaH lines, we can jointly constrain these effects and the low-mass end of the IMF in integrated optical-light spectra of distant ETGs.

### 3 SSP MODELS

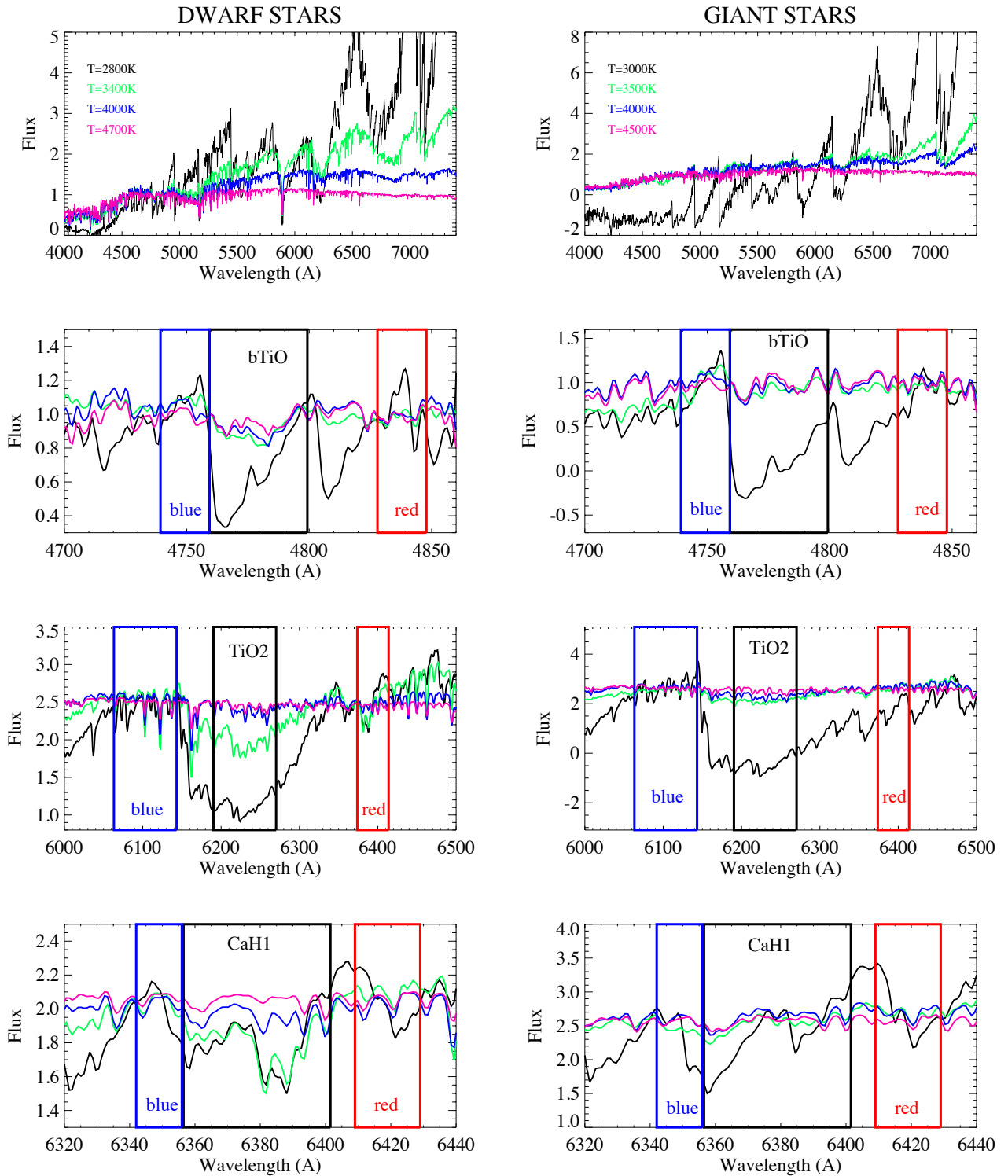
After the recent suggestion by vDC2010 that the low-mass end of the IMF slope may be not universal and might depend on the stellar mass of the system (Treu et al. 2010; Spiniello et al. 2011, 2012; Cappellari et al. 2012, CvD12), new SSP models with varying IMFs have been developed. One of these is CvD12, who presented SSP models with variable abundance patterns and stellar IMFs suitable for studying the integrated-light spectra of galaxies with ages  $> 3$  Gyr. CvD12 synthesized stellar atmospheres and spectra using the combination of three different isochrones to describe separate phases of stellar evolution: the Dartmouth isochrones (Dotter et al. 2008) for the main sequence and the red giant branch (RGB); the Padova isochrones (Marigo et al. 2008) to describe AGB evolution and the horizontal branch (HB); and the Lyon isochrones (Chabrier & Baraffe 1997; Baraffe et al. 1998) for the lower-mass main sequence ( $M_{\star} \leq 0.2 M_{\odot}$ ). All of the CvD12 models use *solar* metallicity isochrones, even when synthesizing with different abundance patterns or different  $[\alpha/\text{Fe}]$ .

The models are based on empirical stellar libraries, modified using theoretical stellar atmosphere models and their emergent synthetic spectra, and therefore they are somewhat restricted in their SSP parameter coverage (especially at high metallicity and for non-solar abundance ratios) and poorly-calibrated against mass loss in advanced stages, such as the asymptotic giant branch (AGB). Stars in these phases provide a non-negligible contribution to the red spectrum of galaxies (Worthey 1994). This contribution is however hard to quantify because RGBs and AGBs are so short-lived that good statistics are hard to obtain from color-magnitude diagrams of globular and open clusters. Moreover, mass loss, which is a crucial ingredient to calculate the precise evolutionary path of AGB, is very hard to model and therefore is a main source of uncertainties in the models (e.g. Blöcker 1995).

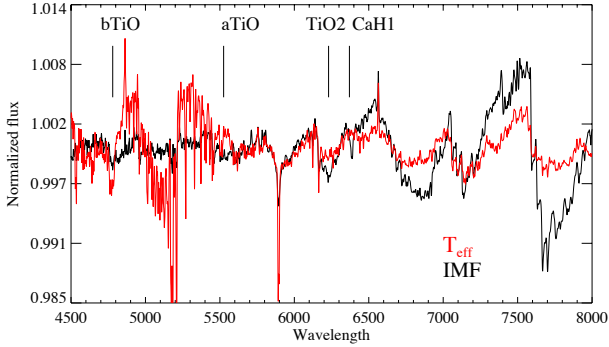
The CvD12 models explore variations in age in the range 3–13.5 Gyr,  $\alpha$ -enhancement of 0–0.4 dex, individual elemental abundance variations and four different IMFs: a bottom-light Chabrier (2003) IMF, a Salpeter (1955) IMF with a slope of  $x = 2.35$  (where  $x$  is the IMF slope, using  $dN/dm \propto m^{-x}$ ), and two bottom-heavy IMFs with slopes of  $x = 3.0$  and  $x = 3.5$ .

Figure 5 shows index strengths versus IMF slope for different ages (different colors) and  $[\alpha/\text{Fe}]$  (symbols) for a number of features from the CvD12 SSP models. Most of the classical blue Lick indices (e.g.  $H\beta$ ,  $[\text{MgFe}]$ : González 1993; Worthey 1994; Trager et al. 2000a) do not show a strong variation with the IMF slope, although they are important in constraining the age and metallicity of galaxies. Index strengths of the newly defined bTiO and aTiO and the redder TiO indices clearly increase with steeper IMF slopes, but they also increase for higher  $[\alpha/\text{Fe}]$ . On the other hand, the CaH1 index strength decreases with increasing  $[\alpha/\text{Fe}]$ . This makes the combination of TiO lines and CaH1 absorption a very good IMF probe, as the effects of  $[\alpha/\text{Fe}]$  and varying IMF slope are orthogonal in a TiO-CaH plot.

We note that other models, such as Thomas et al. (2011), do not find a strong sensitivity of the TiO indices to  $[\alpha/\text{Fe}]$ . The reason why previous models for TiO indices differ from CvD12 is that the old response functions (including



**Figure 3.** *Left panels:* Individual MILES dwarf stars with similar surface gravities ( $\log g \sim 5$ ) and different  $T_{\text{eff}}$ . *Right panels:* Individual MILES giants with similar surface gravities ( $\log g \sim 0.5$ ) and different  $T_{\text{eff}}$ . In the bottom three rows, we show a zoom into different absorption feature regions. Red and blue boxes are the blue and red pseudo-continua bands of the indices. Both bTiO and TiO2 absorption are stronger in cool stars but are present in both dwarfs and giants. The CaH1 index instead only comes from cool dwarfs.



**Figure 4.** Relative effect on the spectrum of IMF and  $T_{\text{eff}}$  variations. Blueward of  $\sim 7500$  Å the effects are almost perfectly degenerate while they decouple redward of TiO2 and CaH1. The response of the two curves however is different around specific features. This makes their combination a powerful tool to decouple the variations.

Korn, Maraston & Thomas 2005, used in e.g., Thomas et al. 2011) do not include TiO molecules, so they will not be able to reproduce the TiO sensitivities.

The dependence on age of index strengths is smaller for almost all the indicators if we restrict ourself to ages  $\geq 7$  Gyr. A caveat of our analysis is that the response functions of CvD12 do not currently include the CaH molecule. However observations of Ca indices indicate a nearly solar  $[\text{Ca}/\text{Fe}]$  abundance in galaxies (Vazdekis et al. 1997; Worthey 1998; Trager et al. 1998; Cenarro et al. 2003; Smith et al. 2009) and therefore this limitation in the response functions is unlikely to impact our results.

#### 4 CONSTRAINING THE LOW-MASS END OF THE IMF SLOPE USING OPTICAL SPECTRA OF ETGS

We now compare the CvD12 models to early-type galaxies (ETGs), for which they are specifically designed.

We selected ETGs from the Sloan Digital Sky Survey DR8 (SDSS; Aihara et al. 2011) in five velocity-dispersion bins spread over  $150\text{--}310\text{ km s}^{-1}$ , each with a total width of  $\sim 40\text{ km s}^{-1}$ . To select ETGs and to minimize contamination of our sample by late-type galaxies, we select systems for which the galaxy’s surface brightness profile has a likelihood of a de Vaucouleurs’ model fit higher than the likelihood of an exponential model fit. This requirement reduces approximately to requiring that the surface brightness profile should be better fitted by the de Vaucouleurs’ model than by an exponential. We also visually inspected spectra of all the selected galaxies removing that showing emission lines (specifically, all the cases in which  $H\beta$ , O[III] or O[II] emission is visible). Moreover, we select systems with very low star-formation rate ( $\text{SFR} < 0.3 M_{\odot} \text{ yr}^{-1}$ ) using the MPA/JHU value-added galaxy catalog containing results from the galaxy spectral fitting code described in Tremonti et al. (2004) and star formation rates based on the technique discussed in Brinchmann et al. (2004). Finally we set an upper limit on the redshift range ( $z \leq 0.05$ ) to cover the entire wavelength range of interest. In each bin we

stack spectra together in order to increase the final signal-to-noise (S/N), which is of the order of  $\sim 300/\text{Å}$  over the wavelength range  $4000\text{--}7000$  Å. We use CvD12 models with varying IMF slopes, ages =  $[7\text{--}13.5]$  Gyr,  $[\alpha/\text{Fe}] = [0, 0.2]$ , and solar abundances. We convolve the galaxy and model spectra to an effective velocity dispersion of  $\sigma = 350\text{ km s}^{-1}$  to correct for kinematic broadening before measuring indices. We also normalize the spectra using a second-order polynomial fit. In Figure 6, we show the stacked SDSS spectra for each velocity dispersion bin as well as a set of models with solar  $[\alpha/\text{Fe}]$  and varying IMF slope. Boxes show the IMF-sensitive indices used in this work.

We measure line-strength indices in the range  $4000\text{--}7400$  Å, including the standard Lick indices  $H\beta$ ,  $Mgb$ ,  $\text{Fe}5270$ ,  $\text{Fe}5335$ ,  $\text{NaD}$  and  $\text{TiO}2$  (e.g., Trager et al. 1998), and the commonly-used  $[\text{MgFe}]$  combination<sup>1</sup>, as well as our newly defined IMF-sensitive features bTiO, aTiO and CaH1. Indices in both the galaxy and the model spectra are measured with the same definitions and methods<sup>2</sup>. We do not place our indices on the zero-point system of the Lick indices and quote the new TiO and CaH indices as index strengths in units of magnitudes. Index-measurements for the stacked spectra of SDSS galaxies in the five velocity-dispersion bins are reported in Table 2.

To investigate the IMF variation with galaxy mass, we produce index-index plots for the selected optical indicators. Panel (a) of Figure 7 shows the  $H\beta\text{--}[\text{MgFe}]$  diagram, used to constrain age and metallicity of galaxies. The different colors represent CvD12 SSP models with different ages and solar  $[\alpha/\text{Fe}]$ . We observe an increase in age with increasing velocity dispersion, consistent with previous stellar population studies of early-type galaxies that suggest that more massive galaxies predominantly have older, more evolved, stellar populations (e.g. Renzini 2006). The reader might notice that contrary to many other SSP models (Worthey 1994; Bruzual & Charlot 1993, 2003; Leitherer et al. 1999; Vazdekis et al. 1996, 1997; Maraston 2005; Thomas et al. 2005), in the CvD12 models the  $[\text{MgFe}]$  index depends on  $[\alpha/\text{Fe}]$ . This is because in the CvD12 models the abundance variations of single elements are implemented at fixed  $[\text{Fe}/\text{H}]$ <sup>3</sup>. All selected galaxies are consistent with populations of 9 Gyr or older, and therefore in the other panels we only plot SSP models with ages of 9, 11, 13.5 Gyr. We plot

<sup>1</sup>  $[\text{MgFe}] = \sqrt{(\text{Fe}5270 + \text{Fe}5335)/2} \times Mgb$ , González (1993)

<sup>2</sup> We use the code SPINDEX from Trager, Faber & Dressler (2008)

<sup>3</sup> Schiavon (2007) has already seen the same effect in his models which have also been cast in terms of  $[\text{Fe}/\text{H}]$ , and not total metallicity  $[\text{Z}/\text{H}]$ . This reflects the choice to deal explicitly with quantities that can be inferred from measurements taken in the integrated spectra of galaxies. Total metallicity is not one of them, given our current inability to use integrated spectra of stellar populations to constrain the most abundant of all metals, oxygen. As clearly discussed in Graves & Schiavon (2008), an advantage with casting models in terms of  $[\text{Fe}/\text{H}]$  is that each elemental abundance can be treated separately, so that the effect of its variation can be studied in isolation from every other elemental abundance at the cost, however, of varying the total metallicity. In the case of models cast in terms of  $[\text{Z}/\text{H}]$ , it is impossible to vary the abundance of a single element, because enhancing one element means decreasing the abundances of all other elements to keep the total metallicity constant.

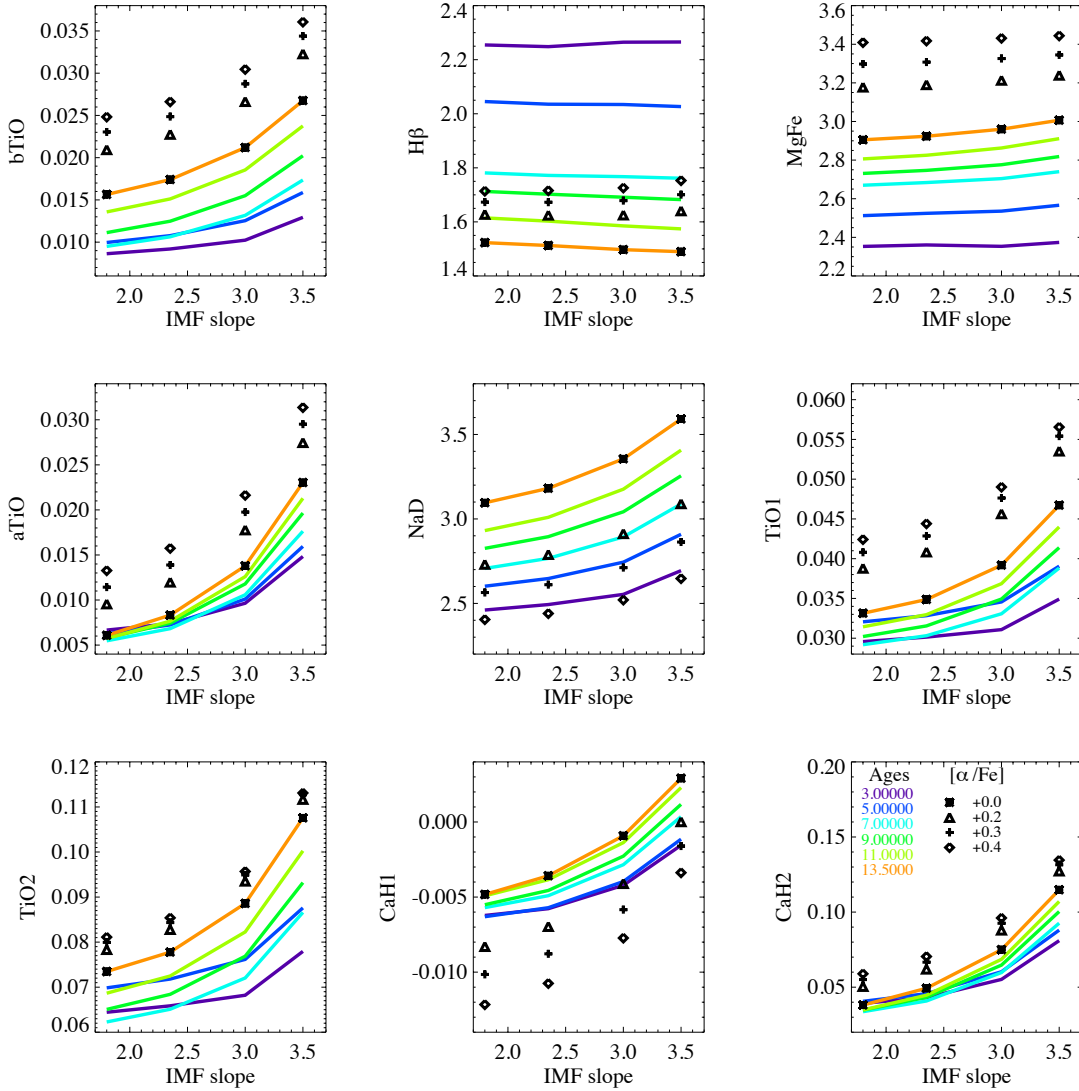


**Figure 5.** Variation of index strengths with IMF slope for CvD12 models in the MILES wavelength range and with a resolution of  $\sigma = 350 \text{ km s}^{-1}$ . In each panel, different colors represent SSP models with different ages, while different symbols are SSP models with an age of  $\sim 13.5$  Gyr and with different  $[\alpha/\text{Fe}]$  ratios. The models predict a generally weak dependence of TiO features on age and an increase of all TiO strengths with increasing IMF. The CaH1 index strength also increases with steepening IMF and age but decreases with increasing  $[\alpha/\text{Fe}]$ . In all plots, a Salpeter IMF (Salpeter 1955) has a slope of  $x = 2.35$ .

models with solar  $[\alpha/\text{Fe}]$  (solid lines) and supersolar  $[\alpha/\text{Fe}]$  ( $= 0.2$  dex, dotted lines); we note that the predicted variation of IMF slopes is orthogonal to the  $[\alpha/\text{Fe}]$  enrichment for the selected IMF-sensitive indicators (Spiniello et al. 2012). Panels (b), (c) and (d) of Figure 7 show some of our selected IMF indicators in the optical. In each panel we plot one of the TiO lines against CaH1, which is the only feature that is strong only in cool dwarfs. The combination of TiO lines (whose strengths increase with steepening of the IMF and with increasing  $[\alpha/\text{Fe}]$ ) and CaH1 absorption (whose index strength instead decreases with increasing  $[\alpha/\text{Fe}]$ ) allows us to break the IMF slope– $[\alpha/\text{Fe}]$  degeneracy. Several TiO lines are necessary to further break the IMF– $T_{\text{eff,RGB}}$ , as described below.

Remarkably, all indicators clearly show a steeper IMF slope with increasing galaxy mass: they imply a

Chabrier IMF for the least-massive galaxies ( $\langle\sigma_*\rangle \sim 150 \text{ km s}^{-1}$ ), Salpeter for the intermediate-mass galaxies ( $\langle\sigma_*\rangle \sim 230 \text{ km s}^{-1}$ ) and possibly a bottom-heavy IMF with  $x \lesssim 3$  for the most massive SDSS ETGs ( $\langle\sigma_*\rangle \sim 310 \text{ km s}^{-1}$ ). We quantify this further in section 4.3.

#### 4.1 Variation in the $\Delta T_{\text{eff}}$ of the red-giant branch versus IMF variations

Here we investigate further the IMF– $\Delta T_{\text{eff,RGB}}$  degeneracy, showing that the data are consistent with a non-universal IMF even when we take into account the possible uncertainty on the exact temperature of the red giant branch in ETGs. We use 13.5 Gyr old CvD12 models in which we change the temperature of the RGB in the isochrones. In each index-index plot of Figure 8 we show the standard-

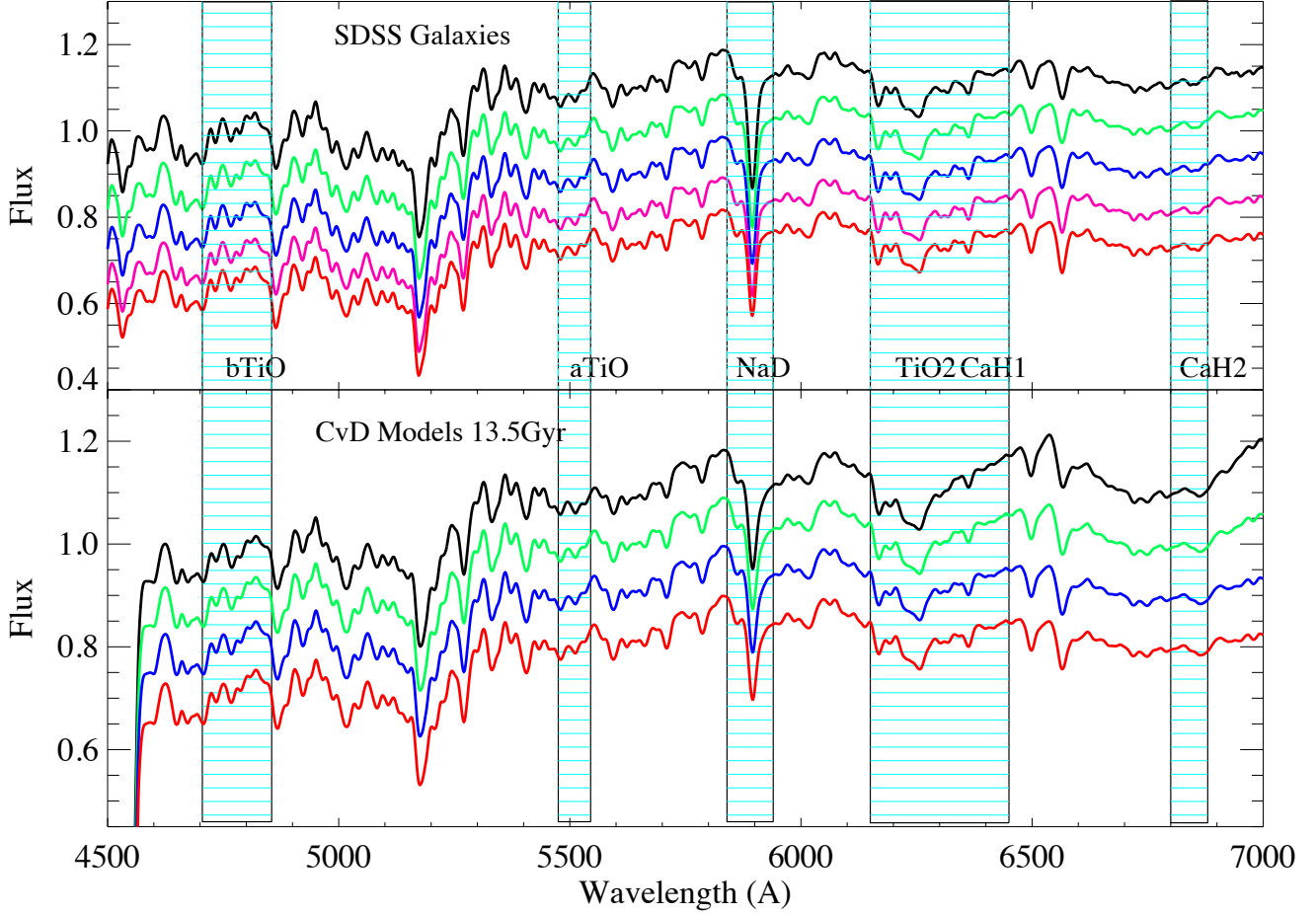


**Figure 6.** *Upper panel:* Stacked spectra of SDSS galaxies with different observed velocity dispersions, increasing from bottom to top (150, 190, 230, 270, 310  $\text{km s}^{-1}$  respectively) and offset for clarity. *Lower panel:* CvD12 SSP models with same age (13.5 Gyr) and solar  $[\alpha/\text{Fe}]$  but different IMF slopes, from Chabrier (at the bottom) to the most bottom-heavy ( $x = 3.5$ , at the top). Boxes show IMF-sensitive features. All observed and model spectra are normalized with a polynomial fitting and convolved to a common resolution of  $\sigma = 350 \text{ km s}^{-1}$ .

**Table 2.** Equivalent widths of the features used in the following analysis for the stacked spectra of SDSS galaxies in the five velocity-dispersion bins with a total width of  $40 \text{ km s}^{-1}$  ( $\Delta\sigma = \pm 20 \text{ km s}^{-1}$ ). The bins have similar number of galaxies: 51, 54, 50, 49, 43 from the lowest to the highest velocity-dispersion bin. The first five line-indices ( $H_\beta$ , Mgb, Fe5270, Fe5335, and NaD) are measured in angstrom, the others in magnitudes.

Index	$EW_{\sigma_* = 150 \text{ km s}^{-1}}$	$EW_{\sigma_* = 190 \text{ km s}^{-1}}$	$EW_{\sigma_* = 230 \text{ km s}^{-1}}$	$EW_{\sigma_* = 270 \text{ km s}^{-1}}$	$EW_{\sigma_* = 310 \text{ km s}^{-1}}$
$H_\beta$	$1.666 \pm 0.001$	$1.523 \pm 0.001$	$1.449 \pm 0.004$	$1.496 \pm 0.003$	$1.491 \pm 0.008$
Mgb	$3.531 \pm 0.001$	$3.878 \pm 0.001$	$4.088 \pm 0.004$	$4.155 \pm 0.003$	$4.282 \pm 0.008$
Fe5270	$2.364 \pm 0.001$	$2.389 \pm 0.001$	$2.400 \pm 0.005$	$2.466 \pm 0.004$	$2.499 \pm 0.010$
Fe5335	$1.768 \pm 0.001$	$1.784 \pm 0.002$	$1.889 \pm 0.006$	$1.803 \pm 0.005$	$1.895 \pm 0.012$
NaD	$3.308 \pm 0.001$	$3.9238 \pm 0.0001$	$4.413 \pm 0.003$	$4.628 \pm 0.003$	$4.962 \pm 0.007$
bTiO	$0.01589 \pm 0.00004$	$0.01936 \pm 0.00004$	$0.0205 \pm 0.0002$	$0.0207 \pm 0.0001$	$0.0212 \pm 0.0003$
aTiO	$0.00839 \pm 0.00002$	$0.01153 \pm 0.00003$	$0.0126 \pm 0.0001$	$0.0114 \pm 0.0001$	$0.0387 \pm 0.0002$
TiO1	$0.03141 \pm 0.00002$	$0.03664 \pm 0.00002$	$0.0390 \pm 0.0001$	$0.39913 \pm 0.0001$	$0.0387 \pm 0.0002$
TiO2	$0.07508 \pm 0.00002$	$0.0815 \pm 0.00002$	$0.08364 \pm 0.0001$	$0.0880 \pm 0.0001$	$0.0900 \pm 0.0002$
CaH1	$-0.00532 \pm 0.00002$	$-0.00467 \pm 0.00003$	$-0.0042 \pm 0.0001$	$-0.0033 \pm 0.0001$	$-0.0321 \pm 0.0002$
CaH2	$0.03471 \pm 0.00002$	$0.03503 \pm 0.00002$	$0.0368 \pm 0.0001$	$0.0349 \pm 0.0001$	$0.0359 \pm 0.0002$

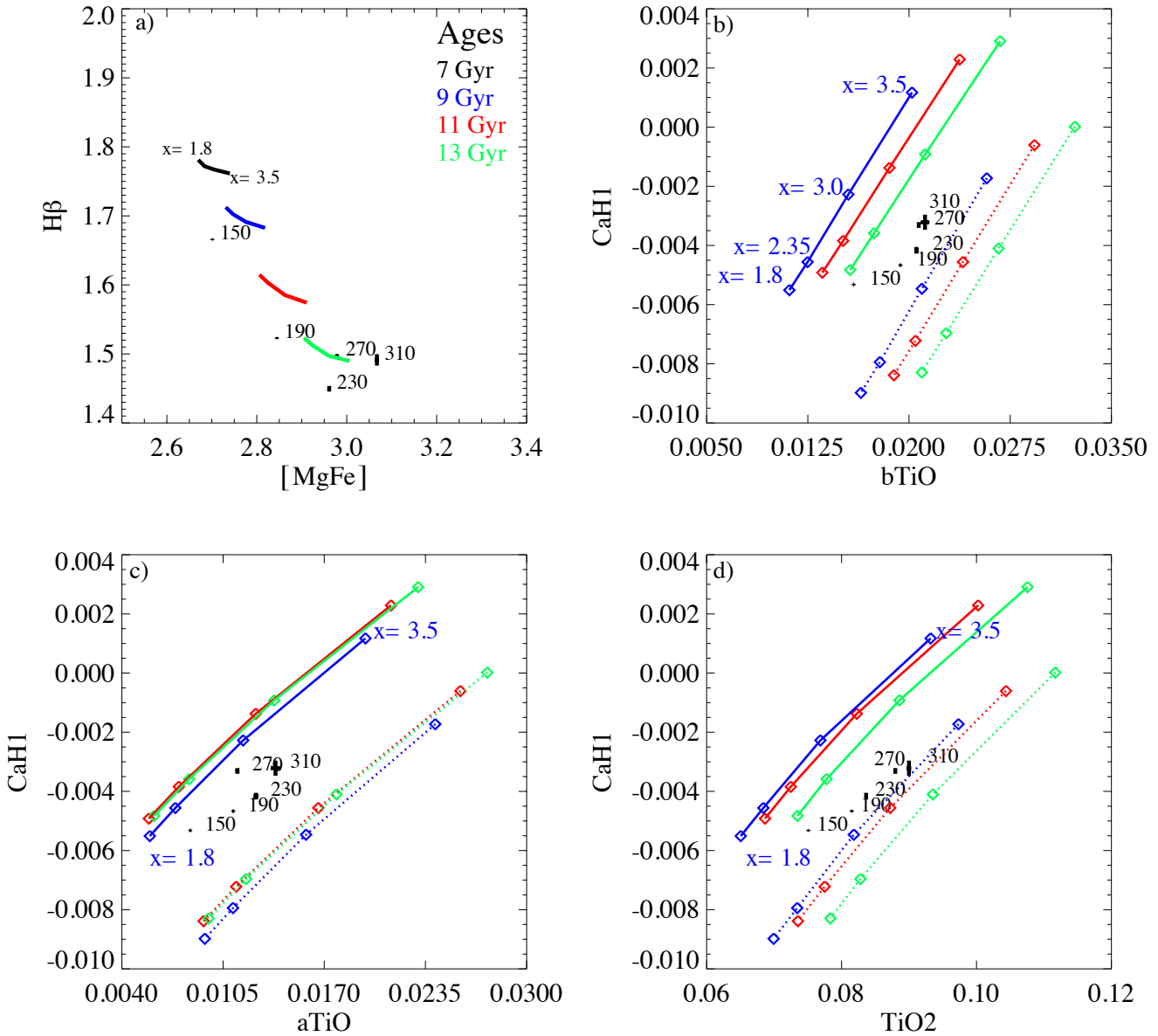


**Figure 7.** Index-index plots of the main absorption features in the optical. Solid lines are CvD12 models with different ages (colors) and different IMF slopes (points on each line are models with IMF slopes of 1.8, 2.35, 3.0, 3.5). Dotted lines are the same models with  $[\alpha/\text{Fe}] = +0.2$  dex. All models have solar metallicity (i.e.,  $[\text{Fe}/\text{H}] = 0.0$ ). Points with error bars are stacked spectra of SDSS galaxies, in five velocity-dispersion ( $\sigma_*$ ) bins. The value shown is the average  $\sigma_*$  in  $\text{km s}^{-1}$  for each bin. Galaxies and models are convolved to a final common resolution of  $350 \text{ km s}^{-1}$  before measuring index strengths. *Panel (a)*: The  $H\beta$ – $[\text{MgFe}]$  diagram. In this plot IMF dependence is minimal, and the ages and metallicities of the galaxies can be inferred. All the galaxies show populations older than 9 Gyr. *Panels (b, c, d)*: IMF-sensitive index-index plots; CaHI as a function of bTiO, aTiO and TiO2 respectively. The TiO lines are strong in cool giants and dwarfs and become strong with increasing  $[\alpha/\text{Fe}]$ . CaHI comes only from M dwarfs and becomes weaker for super-solar  $[\alpha/\text{Fe}]$ . The combination of these indices is therefore particularly effective at constraining the low-mass end of the IMF slope. All the indicators agree and confirm a steepening of the IMF slope with galaxy mass. In these panels, galaxies prefer models with slightly super-solar  $[\alpha/\text{Fe}]$ .

temperature model with solar and super-solar  $[\alpha/\text{Fe}]$ , a solar-abundance model with  $\Delta T_{\text{eff,RGB}}$  increased by 50 K, and three solar-abundance models with  $\Delta T_{\text{eff,RGB}}$  decreased by respectively 50 K, 100 K, and 150 K. On each line, different symbols indicate different assumed IMFs. Figure 8 clearly shows that the combination of our preferred optical IMF-dependent indicators allows us to break also the IMF– $\Delta T_{\text{eff,RGB}}$  degeneracy. It is also clear from the figure that ETGs are slightly  $\alpha$ -enhanced, and that the degeneracy be-

tween IMF,  $\Delta T_{\text{eff,RGB}}$  and  $[\alpha/\text{Fe}]$  can be completely broken by using several TiO lines in combination with the CaHI feature.

In principle the NaD index at  $5900 \text{ \AA}$  could be used to constrain the IMF (Conroy & van Dokkum 2012b; Ferreras et al. 2013), but, as shown in panel (f) of Figure 8, this index is more sensitive to variation of the effective temperature of the RGB stars than to variation of the IMF slope

in these models. However, this feature is above all sensitive to  $[\text{Na}/\text{Fe}]$  abundance, as we will show in the next section.

## 4.2 The Na features

NaD and NaI indices are both very strong absorption features in the optical-NIR spectrum and have been the subject of numerous studies of the IMF slope as well as of the interstellar medium (ISM). The first claim of a non-universal low-mass end of the IMF was made by Spinrad & Taylor (1971) using the NaI feature ( $\lambda \sim 8190 \text{ \AA}$ ). They compared the observed line strength of the NaI doublet in the centers of M31, M32 and M81 with population synthesis models, finding a substantial fractional contribution by dwarf stars to the integrated light of these galaxies. More recently, van Dokkum & Conroy (2010) demonstrated indeed that the NaI doublet depends strongly on surface gravity at fixed effective temperature, betraying the presence of faint M dwarfs in integrated light spectra. Figure 2 shows that the bluer NaD feature ( $\lambda \sim 5900 \text{ \AA}$ ) is also very strong in dwarf stars at relatively low temperatures ( $T_{\text{eff}} \leq 4200\text{K}$ ). Hence, its strength as a function of the redder sodium feature should provide a powerful means for separating the IMF from the sodium abundance, assuming that the two features react in the same way to changes in the  $[\text{Na}/\text{Fe}]$  abundance. However, it has been argued that the NaD index could be highly contaminated by the ISM, even though the dominant process is under great debate (cool gas in the disk, galactic wind in actively star-forming galaxies or AGN activity are the most common candidates, e.g. Heckman, Armus & Miley 1990; Lehnert et al. 2011).

Here we show that the NaD strength is not *solely* driven by IMF variation: we find that this index is more sensitive to  $[\text{Na}/\text{Fe}]$  abundance variations than to IMF slope variations (Spiniello et al. 2013b, in prep.), and it varies strongly with  $T_{\text{eff,RGB}}$ . In Spiniello et al. (2012) we show that CvD12 models with solar  $[\text{Na}/\text{Fe}]$  abundance do not match the NaD strengths for high-mass ETGs. This is also confirmed by Conroy & van Dokkum (2012b) who find that massive ETGs require models with  $[\text{Na}/\text{Fe}] = 0.3\text{--}0.4$ . When *only* sodium indicators are used these systems require also extremely steep IMFs,  $x \geq 3.5$ . For the gravitational lens analysed in Spiniello et al. (2012) paper (with  $\sigma_* \sim 300 \text{ km s}^{-1}$ ), such steep slopes are ruled out at the 99.9 per cent confidence level (C.L.) from lensing constraints. We therefore conclude that Na lines are highly sensitive to both IMF variation and  $[\text{Na}/\text{Fe}]$  variation, and are therefore complicated to interpret when considered in isolation.

Furthermore, in a recent paper, Smith & Lucey (2013) found a giant elliptical ( $\sigma_* \sim 330 \text{ km s}^{-1}$ ) lens galaxy with a “lightweight” IMF. From their lensing analysis, an IMF heavier than Salpeter is disfavoured at the  $> 99.8$  per cent level. However, when looking at the dwarf-sensitive NaI feature in the spectrum of that galaxy, a SSP with age of 13.5 Gyr, super-solar  $[\alpha/\text{Fe}]$  and bottom-heavy IMF ( $x = 3.0$ ) is required to match the observed galaxy spectrum. Also in this case, the stellar mass inferred from this SSP model violates the limits on the total mass of that particular system, set by gravitational lensing. Even when considering models with an enhancement of sodium, Smith & Lucey (2013) cannot completely reconcile the SSP Na-based result and

the lensing result on the IMF slope *for this* particular giant elliptical.

Additional evidence showing that the NaD strengths in ETGs are not exclusively IMF-driven is provided by Jeong et al. (2013). These authors identified NaD excess objects (NEOs) from the SDSS DR7 (Abazajian et al. 2009) and found that NaD features are too strong in many massive ETGs even when using SSP models with a bottom-heavy IMFs (and solar abundance). They studied a plausible range of stellar parameters (from CvD12 SSP models) that could reproduce the observed values of NaD, Mgb and Fe5270, finding that the majority of the early-type NEOs are  $\alpha$ -enhanced, metal-rich and especially Na-enhanced ( $[\text{Na}/\text{Fe}] \sim 0.3$ ).

To further complicate this situation, we note that large differences exist when comparing the behaviour of Na features predicted from different SSP models, as pointed out in La Barbera et al. (2013). The authors compared the  $[\alpha/\text{Fe}]$  sensitivity of the NaD for different SSP models finding a strong discrepancy. They showed that the CvD12, Coelho et al. (2007) and Cervantes et al. (2007) models predict that NaD weakens as  $[\alpha/\text{Fe}]$  increases, while the Thomas et al. (2011) models predict a mild increase with enhancement.

Given this unresolved situation about the level of sodium abundance in ETGs, we therefore think that it is currently prudent not to draw any strong conclusion about the low-mass end of the IMF slope based *solely* on Na features, and to concentrate on indices such as those from TiO and CaH, which appear to be less subject to abundance-ratio variation effects and give mutually consistent predictions for the trend of IMF slope with galaxy mass.

In the following section we give a quantitative expression for the relation between IMF slope and velocity dispersion, showing that the relation inferred from sodium lines is systematically different than the relation inferred from any other combination of the above-mentioned IMF-sensitive spectral indices.

## 4.3 IMF slope versus velocity dispersion

Our results confirm that it is possible to constrain the low-mass end of the IMF slope from optical spectra of ETGs and provide increasing support to the emerging notion of the non-universality of the IMF. We observe that the steepness of the low-mass end of the IMF increases with galaxy velocity dispersion, consistent with previously-published works (van Dokkum & Conroy 2010; Spiniello et al. 2011, 2012; Conroy & van Dokkum 2012b; Cappellari et al. 2012; Ferreras et al. 2013; Tortora, Romanowsky & Napolitano 2013; La Barbera et al. 2013). To constrain the IMF slope of each galaxy and concurrently break the degeneracies between age, metallicity, abundance ratio and temperature, we use the following indices:  $\text{H}\beta$ , Mgb, Fe5270, Fe5335, bTiO, aTiO, TiO1, TiO2, CaH1, and CaH2. The first four indicators are almost IMF-independent and they are mainly used to constrain age and  $[\alpha/\text{Fe}]$ , while the combination of CaH1 with TiO features is used to count dwarfs stars and to break the degeneracy with effective temperature (see Figs. 7 and 8). We also test the effect of including or not the NaD index.

We now give a quantitative expression for the variation of the IMF slope with velocity dispersion. We compare each stacked SDSS spectrum with grids of interpolated SSPs

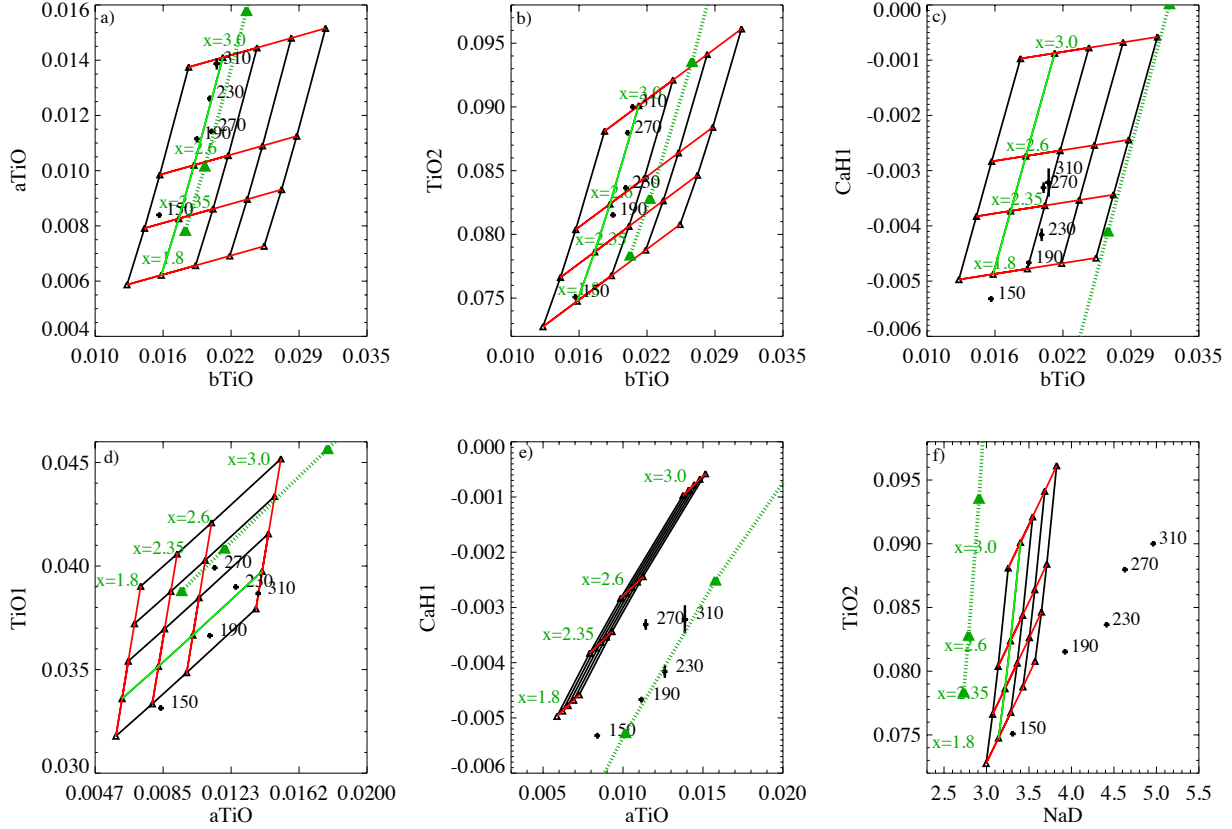


**Figure 8.** The effect of  $\Delta T_{\text{eff,RGB}}$  on CvD12 models with ages of 13.5 Gyr. In each panel, the green solid line shows the standard-temperature model with solar  $[\alpha/\text{Fe}]$  while the black lines are models in which  $\Delta T_{\text{eff,RGB}}$  has been increased or decreased by 50 K. The green dotted line shows the standard-temperature model with  $[\alpha/\text{Fe}] = +0.1$ . We plot models with  $\Delta T_{\text{eff,RGB}} = 50 \text{ K}, -50 \text{ K}, -100 \text{ K}$  and  $-150 \text{ K}$ . Red lines represent therefore  $\Delta T_{\text{eff,RGB}}$  variations, while different symbols on the same black line indicate different IMF slopes for a model with a given temperature. Points with error bars are stacked spectra of SDSS galaxies, in five velocity-dispersion ( $\sigma_*$ ) bins whose average is shown in  $\text{km s}^{-1}$ . *Panels a–d*): The combination of these indicators allow the degeneracy between RGB temperature and IMF to be broken. A mild variation of  $\Delta T_{\text{eff,RGB}}$  with galaxy mass can be detected, but a clear trend of increasing IMF with galaxy mass is present in all three panels. *Panel e*):  $\text{CaH1}$ – $a\text{TiO}$  does not allow simultaneous constraints on the IMF slope and  $\Delta T_{\text{eff,RGB}}$ . From this panel it is clear that models with slightly super-solar  $[\alpha/\text{Fe}]$  better fit the data. The same result is also visible in Figure 7 (c) and (d) and is consistent with the best-fit models of Table 3. *Panel f*):  $\text{NaD}$  strengths in the stacked galaxies show a strong variation with galaxy mass. This variation cannot be entirely explained via non-universality of the IMF (Spiniello et al. 2012). The data suggest that  $\text{NaD}$  is highly dependent on the temperature of the RGB.

spanning a range of ages ( $\log(\text{age}) = [0.8 - 1.15]$  Gyr, with a step of 0.01 Gyr),  $[\alpha/\text{Fe}]$  (between  $-0.2$  and  $+0.4$  dex, with a step of 0.05 dex), and changes in the effective temperature of the RGB ( $\Delta T_{\text{eff,RGB}}$  between  $-200 \text{ K}$  and  $50 \text{ K}$ , with a step of 50 K) for different values of the IMF slope ( $x = 1.8 - 3.5$ , with a step of 0.1 in the slope). Using a bspline interpolation, we build a grid of  $8 \times 13 \times 18 \times 9$  models in  $\log(\text{age})$ ,  $[\alpha/\text{Fe}]$ , IMF slope and  $\Delta T_{\text{eff,RGB}}$ , and for each galaxy spectrum we compute the  $\chi^2$  values for different sets of optical indicators as

$$\chi_n^2 = \sum_{ind=1}^k \chi_{ind,n}^2 = \sum_{ind=1}^k \frac{(EW_{ind}^{obs} - EW_{ind,n}^{mod})^2}{\sigma_{EW_{ind}^{obs}}^2}, \quad (1)$$

where  $n$  is the SSP model of interest and  $k$  is the number of indices. We obtain a probability density function (PDF) for each model via the likelihood function  $L \propto \exp(-\chi^2/2)$ .

We then marginalize over age,  $\Delta T_{\text{eff}}$  and  $[\alpha/\text{Fe}]$  to obtain a best-fitting slope of the IMF and its uncertainty ( $1\sigma$  error on the cumulative probability distribution) for each velocity dispersion bin, assuming flat priors on all parameters.

We present our SSP analysis results in Table 3. We plot the percentile deviation of the EWs measured in the stacked SDSS galaxy spectra ( $EW_{\text{SDSS}}$ ) from the values measured in the correspondent SSP best-fit model ( $EW_{\text{BF}}$ ) and Figure 9.

In Figure 11 we show the best-fit IMF slope as a function of central stellar velocity dispersion. We determine the parameters of a linear regression model,  $x = a \times \log \sigma_{200} + b$ , for the stacked SDSS spectra to be

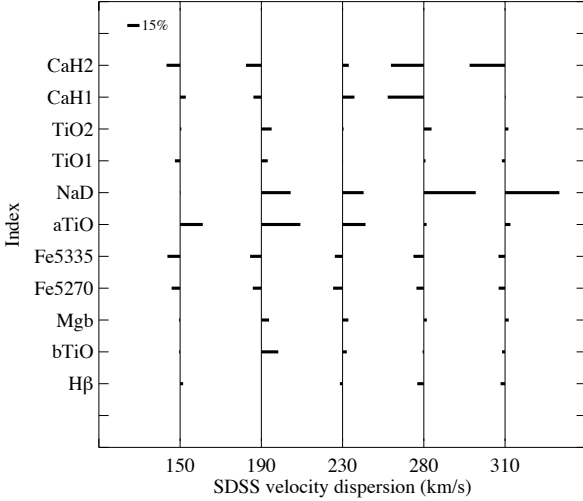
$$x = (2.3 \pm 0.1) \log \sigma_{200} + (2.13 \pm 0.15), \quad (2)$$

when  $\text{NaD}$  is not included and

$$x = (2.6 \pm 0.2) \log \sigma_{200} + (2.3 \pm 0.2), \quad (3)$$

**Table 3.** Best-fit stellar population models for SDSS galaxies in different velocity dispersion bins.  $\Delta T_{\text{eff}}$  shifts are given with respect to the effective temperature of the RGB of solar-scaled models.

SDSS $\sigma_*$ ( $\text{km s}^{-1}$ )	Best-fit age (Gyr)	Best-fit $[\alpha/\text{Fe}]$	Best-fit IMF slope (Salpeter: $x = 2.35$ )	Best-fit $\Delta T_{\text{eff}}$ (K)
$150 \pm 20$	$10 \pm 2$	$-0.11 \pm 0.04$	$1.85 \pm 0.2$	$-50 \pm 30$
$190 \pm 20$	$11 \pm 2$	$+0.05 \pm 0.02$	$2.08 \pm 0.2$	$-98 \pm 36$
$230 \pm 20$	$13 \pm 2$	$+0.11 \pm 0.02$	$2.33 \pm 0.4$	$-115 \pm 29$
$270 \pm 20$	$12 \pm 2$	$+0.16 \pm 0.04$	$2.40 \pm 0.3$	$-80 \pm 30$
$310 \pm 20$	$13 \pm 3$	$+0.14 \pm 0.02$	$2.62 \pm 0.4$	$-131 \pm 40$

**Figure 9.** Deviation of the EWs measured in the stacked SDSS galaxy spectra ( $EW_{\text{SDSS}}$ ) from the values measured in the corresponding SSP best-fit model ( $EW_{\text{BF}}$ ). For each velocity dispersion bin, shown on the  $x$ -axis, the vertical lines indicate the model values of the fitted indices, indicated on the  $y$ -axis. Horizontal lines departing from these indicate the percentile variations of the given index. As reference, we show the length of a line corresponding to a deviation of 15 per cent on the upper-left corner. When the value of the  $EW_{\text{SDSS}}$  is bigger than the value of the  $EW_{\text{BF}}$ , the horizontal line goes to the right, as for NaD. The  $EW_{\text{SDSS}}$  of the NaD feature in the more massive galaxies are systematically underestimated by the SSP models, because we are restricting the analysis to solar  $[\text{Na}/\text{Fe}]$  (see Sec. 4.2).

when using NaD. In the equations  $x$  is the IMF slope and  $\sigma_{200}$  is the central stellar velocity dispersion measured in units of  $200 \text{ km s}^{-1}$ .

To test the robustness of the IMF- $\sigma$  relation, we repeat the above statistical procedure several times eliminating each time one or more indices and calculating a new likelihood function for each model and the inferred stellar population parameters for each stacked spectrum. We always keep  $H\beta$ , our only age-dependent and IMF-independent feature. Our inferred IMF slopes are consistent within  $1\sigma$  if we use CaH1,  $H\beta$ ,  $Mgb$ , at least one of the iron lines, one of the blue TiO indices (bTiO or aTiO) and one of the redder TiO features (TiO1 or TiO2). If we use the  $[\text{Mg}/\text{Fe}]$  as a single indicator we still recover the IMF variation with velocity dispersion, but we do not recover the well-established  $[\alpha/\text{Fe}]$ - $\sigma_*$  relation (Trager et al. 2000a; Arrighi et al. 2010). If we do not include CaH1 we are not able to break the de-

generacy between  $[\alpha/\text{Fe}]$  and IMF slope. In this case, all the IMF-sensitive features increase both with steepening of the IMF slope and increasing of  $[\alpha/\text{Fe}]$ . The aTiO index does not significantly affect the IMF slope if we include or exclude it, confirming that the [OI] sky line does not have a significant effect on the inference of the IMF slope from this absorption feature. However, if we exclude aTiO from the analysis we find RGB effective temperatures systematically higher than those inferred by including aTiO.

The situation changes when NaD is included: the slope of the linear relation becomes significantly steeper when we include this index. In Figure 10 we show this effect by plotting the resulting value of the slope of the linear relation  $x = a \log \sigma_{200} + b$  inferred from different sets of indicators noted in Table 4. We note that we are restricting this particular analysis to solar Na abundances. A trend of increasing  $[\text{Na}/\text{Fe}]$  abundance with galaxy mass can *partially* mimic the IMF steepening. We address this in a forthcoming paper. It is important to note that we are assuming  $[\text{Na}/\text{Mg}] = 0.0$ , which may not be a good assumption for these very massive ETGs. A full spectral fitting approach as in Conroy & van Dokkum (2012b) and Conroy, Graves & van Dokkum (2013) might be necessary to investigate in detail the effect of a single non-solar element abundance.

We note a relation between  $\Delta T_{\text{eff}}$  and  $\sigma$  in Table 3: stacks of the spectra of low- $\sigma$  galaxies show smaller temperature shifts than stacked spectra of high- $\sigma$  galaxies. We believe that the basis for this trend is to be found in a trend between  $\Delta T_{\text{eff}}$  and metallicity or more specifically the overall abundance of  $\alpha$ -elements (i.e., Salaris, Chieffi & Straniero 1993; Pietrinferni et al. 2006; Dotter et al. 2007).

To test whether the trend  $\Delta T_{\text{eff}} - \sigma$  trend has an impact on the IMF- $\sigma$  relation, we repeat the same analysis by fixing  $\Delta T_{\text{eff,RGB}} = 0K$  and  $= -100K$  for the set ID 4 and 9, which give respectively the shallower and the steepest IMF- $\sigma$  relations. When we fix the  $T_{\text{eff,RGB}}$  we still recover the same IMF- $\sigma$  relation within the errors. Best fit ages,  $[\alpha/\text{Fe}]$  and IMF slopes obtained with  $\Delta T_{\text{eff,RGB}} = -100K$  are consistent within  $1 - \sigma$  with the ones obtained by letting the  $T_{\text{eff,RGB}}$  be a free parameter. However the best-fit IMF slopes obtained with solar-scaled  $T_{\text{eff,RGB}}$  are systematically higher, especially for the two most massive bins (set 9 :  $x = 3.3$  for  $\sigma = 310 \text{ km s}^{-1}$  and  $x = 3.3$  for  $\sigma = 270 \text{ km s}^{-1}$ ). The latter result is true for both the chosen sets of indicators and is more extreme for set ID 9. This happens probably because by allowing the temperature of the RGB to be colder, the measured equivalent widths of the gravity-sensitive features will be larger, and therefore the inferred IMF slope will be larger.

**Table 4.** Summary of the parameters of the inferred best-fit IMF slope as a function of central stellar velocity dispersion (though the linear equation  $x = a \log \sigma_{200} + b$ ) using different sets of indices. The first row represents our preferred set. The non-universality of the IMF slope is confirmed in all the tested combinations. However, the trend of the IMF slope with  $\sigma_*$  gets steeper when NaD is used. See the text for further details.

Set ID (see Fig.10)	Used indices	a	b
1	$H\beta$ , Mgb, Fe5270, Fe5335, bTiO, aTiO, TiO1, TiO2, CaH1 and CaH2	$2.3 \pm 0.1$	$2.1 \pm 0.2$
2	$H\beta$ , Mgb, Fe5270, Fe5335, bTiO, aTiO, TiO1, TiO2, CaH1	$2.3 \pm 0.1$	$2.1 \pm 0.2$
3	$H\beta$ , Mgb, Fe5270, Fe5335, bTiO, aTiO, TiO1, TiO2, CaH2	$2.3 \pm 0.2$	$2.1 \pm 0.2$
4	$H\beta$ , Mgb, Fe5270, Fe5335, bTiO, aTiO, TiO1, TiO2	$2.2 \pm 0.3$	$2.3 \pm 0.3$
5	$H\beta$ , Mgb, Fe5270, bTiO, aTiO, TiO1, CaH1	$2.3 \pm 0.3$	$2.1 \pm 0.3$
6	$H\beta$ , Mgb, Fe5270, bTiO, aTiO, TiO2, CaH2	$2.4 \pm 0.3$	$2.2 \pm 0.3$
7	$H\beta$ , Mgb, Fe5270, Fe5335, bTiO, aTiO, TiO1, TiO2, CaH1, CaH2 and NaD	$2.6 \pm 0.2$	$2.3 \pm 0.2$
8	$H\beta$ , Mgb, Fe5270, Fe5335, bTiO, aTiO, TiO1, TiO2, CaH1 and NaD	$2.9 \pm 0.2$	$2.1 \pm 0.1$
9	$H\beta$ , Mgb, Fe5270, Fe5335, bTiO, aTiO, TiO1, TiO2, CaH2 and NaD	$3.2 \pm 0.2$	$2.2 \pm 0.2$
10	$H\beta$ , Mgb, Fe5270, Fe5335, bTiO, aTiO, TiO1, TiO2, and NaD	$3.2 \pm 0.2$	$2.4 \pm 0.2$

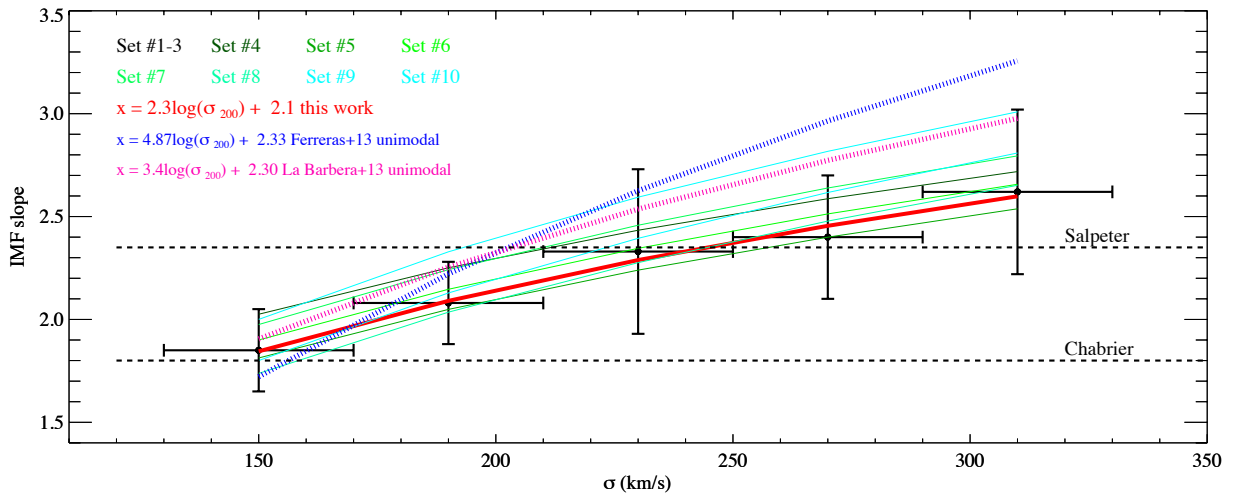


**Figure 11.** Variation of the IMF slope as a function of stellar velocity dispersion. Points are SDSS ETGs stacked by velocity dispersion. The red solid line represents the the IMF- $\sigma_{200}$  relation obtained by using our preferred set of ten indicators, as described in Table 4. The colored lines show the same relation for each set of indicators. The blue dotted line is the linear fit obtained by F13, and the magenta dashed line is the linear fit obtained by LB13 for a unimodal IMF. A very good agreement is found with LB13, when using a similar set of indicators (i.e. including NaD and excluding CaH1). The Chabrier and Salpeter cases are shown as horizontal dashed lines.

#### 4.4 Comparison with other works

In this section we compare our spectroscopic stellar population-based results on the IMF- $\sigma_*$  relation with results obtained from similar SSP-based methods by other authors and from dynamically-based and lensing-based results.

Ferreras et al. (2013, hereafter F13) and La Barbera et al. (2013, hereafter LB13) also found a correlation between central velocity-dispersion and IMF slope for a large sample of SDSS ETGs. F13 combined spectra of  $\sim 40,000$  galaxies in velocity-dispersion bins, obtaining a final set of 18 stacked spectra at very high signal-to-noise ratio ( $S/N \sim 400 \text{ \AA}^{-1}$ ). They compared spectral line strengths sensitive to age, metallicity, and IMF slope of these galaxies with the population synthesis models of Vazdekis et al. (2012). Using TiO1, TiO2 and NaI ( $\lambda 8190 \text{ \AA}$ ), they found  $x = 4.87 \log \sigma_{200} + 2.33$ . Qualitatively the general trends are similar to what we have found above, but their analytical fit has a much steeper slope and therefore predicts a larger variation of the IMF slopes with galaxy mass. For galaxies

with  $\sigma \geq 300 \text{ km s}^{-1}$ , they inferred a very steep IMF slope of  $x \sim 3.2$ . The reason of this apparent discrepancy between our result and that of in F13 appears to be due to the fact that F13 using SSP models with the standard  $T_{\text{eff,RGB}}$  from the isochrones. When using the standard  $T_{\text{eff,RGB}}$  we obtain an IMF- $\sigma$  relation that is consistent within  $1\sigma$  with that of F13.

F13 only used three indicators to constrain the stellar population parameters, two of them coming from TiO lines that are sensitive to  $\alpha$ -enrichment, as shown in our analysis. Disentangling IMF variations from age, metallicity and  $[\alpha/\text{Fe}]$  variations and breaking the degeneracies is very difficult if only a few IMF-sensitive features are used. We therefore believe that our result is more robust because it is based on the combination of more IMF-sensitive indices, and it infers IMF slopes that do not violate lensing constraints on the total masses of massive ETG lenses (see Spiniello et al. 2011, 2012). In fact, LB13 find a relation similar to that we found in this work (within  $1\sigma$ , see Fig. 11) when analysing a

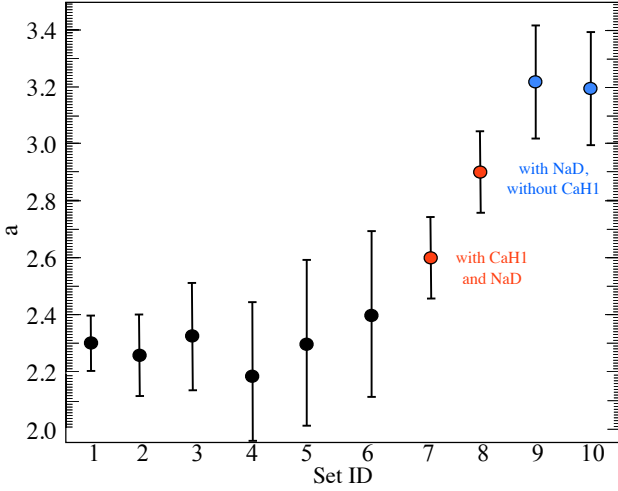


**Figure 10.** The slope of the linear relation  $x = a \log \sigma_{200} + b$  inferred by using the different sets of indices as given in Table 4. The results are robust and stable against systematics arising from single indicators. When using NaD we find a steep relation.

variety of spectral indices, combining IMF-sensitive features with age- and metallicity-sensitive indices and considering the effect of non-solar abundance variations. A very good agreement is found between this work and LB13 when using a similar set of indicators (i.e. including NaD). LB13 and F13 test two different cases of a single power-law (unimodal) and a low-mass ( $< 0.5 M_{\odot}$ ) tapered IMF (bimodal), showing that bimodal IMF shapes do not provide such high  $\Upsilon_{\star}$  ratios even for very steep slopes.

In order to compare our SSP-based results to lensing and dynamics-based results, and our unimodal IMF to the bimodal IMF of LB13, we translate the IMF slope– $\sigma_{\star}$  relation into a  $\Upsilon_{\star}$ – $\sigma_{\star}$  relation. For each SDSS velocity-dispersion bin, we calculate the stellar  $\Upsilon_{\star}$  in the  $R$ -band using the Dartmouth Stellar Evolution Program (Chaboyer et al. 2001), selecting the IMF slope, age, and  $[\alpha/\text{Fe}]$  inferred from the line-strength analysis. We then calculate the ratio of this value and the  $\Upsilon_{\star}$  that the same population (i.e. same age and  $[\alpha/\text{Fe}]$ ) will have assuming a Salpeter IMF (a single power law with  $x = 2.35$ ). In this way, we define an “IMF mismatch” parameter  $\alpha_{\text{IMF}}$ , following an approach similar to the one proposed by Treu et al. (2010) and used by Cappellari et al. (2013):

$$\alpha_{\text{IMF}} = \frac{(\Upsilon)_{\star}^*}{(\Upsilon)_{\text{Salp}}^*}. \quad (4)$$

In Figure 12 we plot  $\log(\alpha_{\text{IMF}})$  as a function of  $\log \sigma_{\star}$  and compute the corresponding linear regression for the SDSS points (black points)

$$\log(\alpha)_{\text{IMF}} = (1.05 \pm 0.2) \log \sigma_{\star} - (2.5 \pm 0.4). \quad (5)$$

Moreover, we show linear fits to the gravitational-lensing-based results of SLACS (blue, Treu et al. 2010) and to stellar population-based results (green: Conroy & van Dokkum 2012b; magenta: La Barbera et al. 2013). Finally we plot the sample of 260 ATLAS3D galaxies (red points, Cappellari et al. 2011, 2013). The linear fit of LB13 is obtained using the linear relation between best-fit slope of the IMF and cen-

tral velocity dispersion given in their Figure 12. We use the mass-to-light ratios in the Johnson  $R$ -band (Vega system) predicted from the MIUSCAT SSP models<sup>4</sup> with an age of 12.6 Gyr, solar metallicity and bimodal IMFs to convert the IMF slope– $\sigma_{\star}$  relation into a  $\Upsilon_{\star}$ – $\sigma_{\star}$  relation. In particular we use the bimodal IMF slopes obtained by fitting spectral indices with two SSP plus X/Fe models. These models consist of a linear combination of two extended MIUSCAT SSPs with the same IMF but different ages and metallicities. In addition, the models incorporate three free parameters describing the  $[\text{Ca}/\text{Fe}]$ ,  $[\text{Na}/\text{Fe}]$ , and  $[\text{Ti}/\text{Fe}]$  abundances.

In Figure 12, we also draw two horizontal lines showing the  $\alpha_{\text{IMF}}$  for a Chabrier-like (single power-law with  $x = 1.8$ ) and a Salpeter IMF (i.e.  $\log(\alpha_{\text{IMF}}) = 0$ ). We note that a bottom-heavy IMF with slope of  $x = 3.0$  falls out of the plot, predicting a value of  $\log(\alpha_{\text{IMF}}) \sim 0.6$ . The good agreement between the stacked SDSS data points and these completely independent analyses (at least at the massive end of the different samples) gives confidence that our spectroscopic analysis and our inferred variation of the IMF slope with velocity dispersion are robust, and the trend we observe depends neither on the SSP model chosen nor on our statistical analysis.

## 5 DISCUSSION AND CONCLUSIONS

In this paper, we have defined a new set of indices which are strong in cool giants and dwarfs and almost absent in main sequence stars, in a spectral region where single-stellar population (SSP) models have been most extensively studied. These features arise from TiO and CaH molecular absorption bands in the wavelength range  $\sim 4700\text{--}7000 \text{ \AA}$ . We have calculated the strengths of these indices for stars in the MILES empirical library. In particular we have shown that all the TiO indicators are strong in cool giants and dwarfs and almost absent in warm main-sequence stars, allowing the study of their variation with temperature, gravity and  $[\text{Fe}/\text{H}]$ . However, the strength of the TiO lines increases with the increasing of the IMF but also with increasing  $[\alpha/\text{Fe}]$ . The feature around CaH1  $\lambda 6380$ , which is strong only in M dwarfs, decreases instead with increasing  $\alpha$ -enhancement and therefore allows us, in combination with the TiO indicators, to break the degeneracy between IMF and  $[\alpha/\text{Fe}]$  variations and thus to constrain the low-mass end of the IMF slope.

We have used the Conroy & van Dokkum (2012a) SSP models constructed specifically for the purpose of measuring the IMF slope down to  $\sim 0.1 M_{\odot}$  for old, metal-rich stellar populations. We have measured SSP index strengths for our new set of IMF indicators, and we have compared these to strengths of stacked spectra of SDSS DR8 ETGs in five different velocity dispersion bins between 150 and  $310 \text{ km s}^{-1}$ . Finally we also investigated in detail the response of a change in the effective temperature of the red giant branch in the isochrones versus the response in variation of the IMF slope for the wavelength range where these responses are shown to be mostly degenerate.

<sup>4</sup> <http://miles.iac.es/pages/photometric-predictions/based-on-miuscat-seds.php>

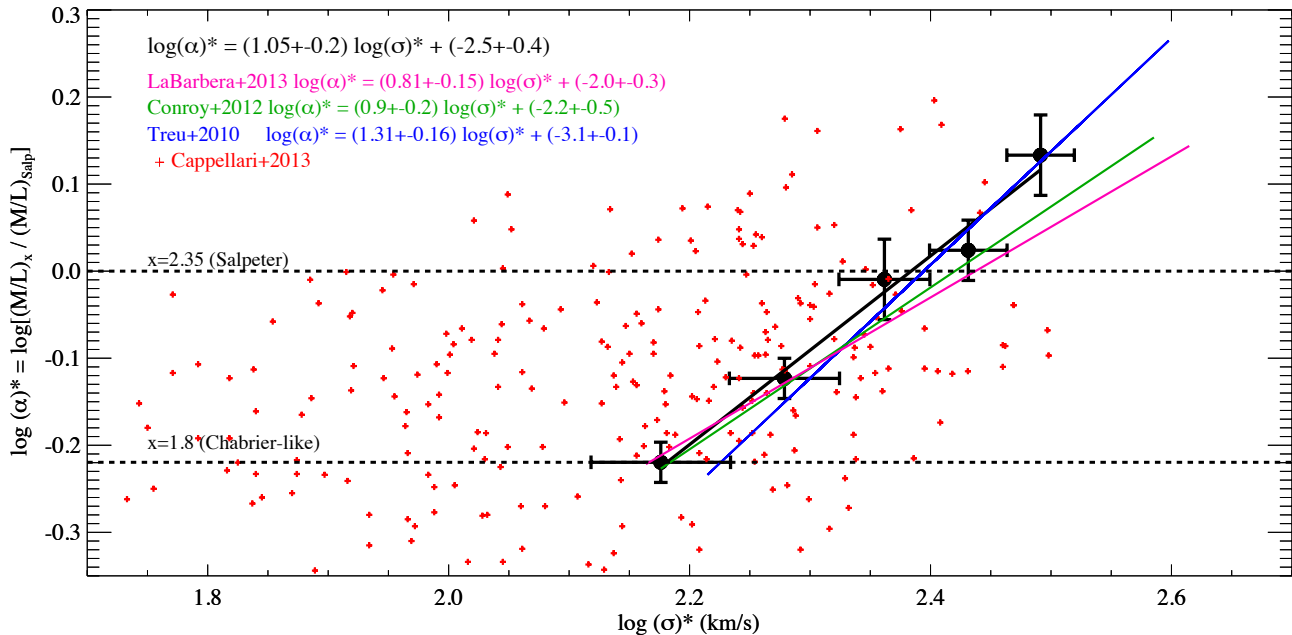


**Figure 12.** The  $\alpha_{\text{IMF}}-\sigma_*$  relation. Our points and their error bars are shown in black, and a linear least-squares fit to these points is shown as the black line. Red points are single galaxies from the ATLAS3D sample. Colored lines are least-squares fits to the  $\alpha_{\text{IMF}}-\sigma_*$  relation derived from the spectroscopic analysis of CvD12b, of LB13 with a bimodal IMF slope, and the lensing+dynamic analysis from Treu et al. (2010). The plot highlights the excellent agreement between these independent studies in their common velocity dispersion range. The Chabrier and Salpeter cases are shown as horizontal dotted lines. A bottom-heavy IMF with slope of  $x = 3.0$  predicts  $\log(\alpha_{\text{IMF}}) \sim 0.6$ .

In this work, we focused only on line-index measurement and we restricted the analysis to solar metallicity. Element abundance is a fundamental parameter that has to be fully and quantitatively explored in order to further isolate and test the suggested variation of IMF normalization with galaxy mass. A full spectral fitting approach can help to further investigate possible IMF variations with galaxy masses and to trace the complete star formation history of a galaxy (Conroy, Graves & van Dokkum 2013).

Our main conclusions are the following.

- CvD12 SSP models predict a minimal variation of the aTiO and CaH1 EWs with age (at least for old ages) and a minimal dependence of  $[\alpha/\text{Fe}]$  on TiO2.
- The predicted variation of IMF slopes is orthogonal to  $[\alpha/\text{Fe}]$  enrichment for all the presented IMF-sensitive index-index plots.
- Our set of IMF-sensitive indicators is able to break the  $\text{IMF}-T_{\text{eff,RGB}}$  degeneracy. The index strengths of SDSS galaxies match better those of SSP models with a population of RGB stars slightly cooler than the default isochrones. However this cannot explain the trend of IMF slope with galaxy velocity dispersion.
- A variation of the IMF with galaxy velocity dispersion, consistent with previous works (Treu et al. 2010; Spiniello et al. 2011, 2012; Cappellari et al. 2012; Tortora, Romanowsky & Napolitano 2013; La Barbera et al. 2013) is visible in all the index-index plots for the SDSS stacked spectra of galaxies in different  $\sigma_*$  bins from 150 to 310  $\text{km s}^{-1}$ . We find  $x = (2.3 \pm 0.1) \log \sigma_{200} + (2.13 \pm 0.15)$  using ten indicators. This result is within  $1\sigma$  of La Barbera et al. (2013),

who performed a detailed analysis using more IMF-sensitive indicators than Ferreras et al. (2013), two SSP models and a correction for the effect of non-solar abundance patterns ( $X/\text{Fe}$ ).

- Our fit predicts an IMF slope that is more shallow than 3.0 for the most massive  $\sigma$ -bin. This is in agreement with the upper limit sets by gravitational lensing studies on the analysis of one very massive lens ETG (Spiniello et al. 2012)
- We translate the  $\text{IMF}-\sigma_{\text{star}}$  relation into a  $\Upsilon_{S_*}-\sigma_*$  relation and compute an “IMF mismatch” parameter ( $\alpha_{\text{IMF}}$ ). This allows us to compare our results with Cappellari et al. (2013), Treu et al. (2010) La Barbera et al. (2013) and Conroy & van Dokkum (2012b). The studies, based on three completely independent methods, and two different SSP models are in excellent agreement.

In conclusion, the newly defined optical IMF indicators bTiO, aTiO, TiO1, TiO2, CaH1, and CaH2, represent useful probes for decoupling the IMF from stellar population age, metallicity, bulk abundance ratio  $[\alpha/\text{Fe}]$ , and the effective temperature of the RGB, when used in combination with age and metallicity indicators. These features are in a region of the spectrum less affected by sky lines or atmospheric absorption lines than the NIR features previously used. This region is also easier to observe as it lies in the wavelength region of the majority of the optical spectrographs, including integral-field instruments, that could be used to spatially resolve the low-mass stellar population of galaxies (Spiniello et al. 2014, in prep.).

In this work, we focussed only on line-index measurements and we restricted our analysis to solar metallicity

and abundances. In this context, results relying primarily on NaD should be treated with some caution. Element abundance is a fundamental parameter that has to be fully and quantitatively explored in order to completely isolate and test the suggested variation of IMF normalization with galaxy mass (in particular [Na/Fe], Spiniello et al., 2013b, in prep.). A full spectral fitting approach might also be necessary to further investigate possible IMF variations with galaxy masses and to trace the complete star formation history of a galaxy (Conroy, Graves & van Dokkum 2013).

## ACKNOWLEDGEMENTS

C.S. acknowledges support from an Ubbo Emmius Fellowship. C.C. acknowledges support from the Alfred P. Sloan Foundation. C.S. thanks Amina Helmi, Gerjon Mensinga, Matteo Barnabè and Gergo Popping for thoughtful comments that have improved the quality of the manuscript. We thank Michele Cappellari, Sukyuong Ken Yi and Hyunjin Jeong for interesting discussions and suggestions. We are grateful to the anonymous referee for his/her insightful and constructive comments. Funding for SDSS-III has been provided by the Alfred P. Sloan Foundation, the Participating Institutions, the National Science Foundation, and the U.S. Department of Energy Office of Science. The SDSS-III web site is <http://www.sdss3.org/>. SDSS-III is managed by the Astrophysical Research Consortium for the Participating Institutions of the SDSS-III Collaboration including the University of Arizona, the Brazilian Participation Group, Brookhaven National Laboratory, University of Cambridge, Carnegie Mellon University, University of Florida, the French Participation Group, the German Participation Group, Harvard University, the Instituto de Astrofísica de Canarias, the Michigan State/Notre Dame/JINA Participation Group, Johns Hopkins University, Lawrence Berkeley National Laboratory, Max Planck Institute for Astrophysics, Max Planck Institute for Extraterrestrial Physics, New Mexico State University, New York University, Ohio State University, Pennsylvania State University, University of Portsmouth, Princeton University, the Spanish Participation Group, University of Tokyo, University of Utah, Vanderbilt University, University of Virginia, University of Washington, and Yale University.

## REFERENCES

- Abazajian K. N. et al., 2009, *ApJS*, 182, 543  
 Aihara H. et al., 2011, *ApJS*, 193, 29  
 Allard F., Hauschildt P. H., Schwenke D., 2000, *ApJ*, 540, 1005  
 Arrigoni M., Trager S. C., Somerville R. S., Gibson B. K., 2010, *MNRAS*, 402, 173  
 Auger M. W., Treu T., Bolton A. S., Gavazzi R., Koopmans L. V. E., Marshall P. J., Moustakas L. A., Burles S., 2010a, *ApJ*, 724, 511  
 Auger M. W., Treu T., Gavazzi R., Bolton A. S., Koopmans L. V. E., Marshall P. J., 2010b, *ApJ*, 721, L163  
 Baraffe I., Chabrier G., Allard F., Hauschildt P. H., 1998, *A&A*, 337, 403  
 Barbuy B., Schiavon R. P., Gregorio-Hetem J., Singh P. D., Batalha C., 1993, *A&A*, Supplement, 101, 409  
 Barnabè M., Czoske O., Koopmans L. V. E., Treu T., Bolton A. S., 2011, *MNRAS*, 415, 2215  
 Bastian N., Covey K. R., Meyer M. R., 2010, *ARA&A*, 48, 339  
 Blöcker T., 1995, *A&A*, 297, 727  
 Blumenthal G. R., Faber S. M., Primack J. R., Rees M. J., 1984, *Nature*, 311, 517  
 Brinchmann J., Charlot S., White S. D. M., Tremonti C., Kauffmann G., Heckman T., Brinkmann J., 2004, *MNRAS*, 351, 1151  
 Bruzual G., Charlot S., 1993, *ApJ*, 405, 538  
 —, 2003, *MNRAS*, 344, 1000  
 Cappellari M. et al., 2011, *MNRAS*, 413, 813  
 —, 2012, *Nature*, 484, 485  
 —, 2013, *MNRAS*, 432, 1862  
 Carter D., Visvanathan N., Pickles A. J., 1986, *ApJ*, 311, 637  
 Cenarro A. J., Cardiel N., Gorgas J., Peletier R. F., Vazdekis A., Prada F., 2001, *MNRAS*, 326, 959  
 Cenarro A. J., Gorgas J., Vazdekis A., Cardiel N., Peletier R. F., 2003, *MNRAS*, 339, L12  
 Cervantes J. L., Coelho P., Barbuy B., Vazdekis A., 2007, in *IAU Symposium*, Vol. 241, *IAU Symposium*, Vazdekis A., Peletier R., eds., pp. 167–168  
 Chaboyer B., Fenton W. H., Nelan J. E., Patnaude D. J., Simon F. E., 2001, *ApJ*, 562, 521  
 Chabrier G., 2003, *PASP*, 115, 763  
 Chabrier G., Baraffe I., 1997, *A&A*, 327, 1039  
 Coelho P., Bruzual G., Charlot S., Weiss A., Barbuy B., Ferguson J. W., 2007, *MNRAS*, 382, 498  
 Cohen J. G., 1978, *ApJ*, 221, 788  
 Conroy C., 2013, *ArXiv e-prints*  
 Conroy C., Graves G., van Dokkum P., 2013, *ArXiv e-prints*  
 Conroy C., van Dokkum P., 2012a, *ApJ*, 747, 69  
 Conroy C., van Dokkum P. G., 2012b, *ApJ*, 760, 71  
 Couture J., Hardy E., 1993, *ApJ*, 406, 142  
 Cushing M. C., Rayner J. T., Vacca W. D., 2005, *ApJ*, 623, 1115  
 Davé R., 2008, *MNRAS*, 385, 147  
 Davis M., Efstathiou G., Frenk C. S., White S. D. M., 1985, *ApJ*, 292, 371  
 Dotter A., Chaboyer B., Ferguson J. W., Lee H.-c., Worthey G., Jevremović D., Baron E., 2007, *ApJ*, 666, 403  
 Dotter A., Chaboyer B., Jevremović D., Kostov V., Baron E., Ferguson J. W., 2008, *ApJS*, 178, 89  
 Dutton A. A., Mendel J. T., Simard L., 2012, *MNRAS*, 422, L33  
 Faber S. M., French H. B., 1980, *ApJ*, 235, 405  
 Ferreras I., La Barbera F., de la Rosa I. G., Vazdekis A., de Carvalho R. R., Falcón-Barroso J., Ricciardelli E., 2013, *MNRAS*, 429, L15  
 Fowler A., 1907, *Royal Society of London Proceedings Series A*, 79, 509  
 Frenk C. S., White S. D. M., Efstathiou G., Davis M., 1985, *Nature*, 317, 595  
 Frogel J. A., Persson S. E., Cohen J. G., 1980, *ApJ*, 240, 785  
 Frogel J. A., Persson S. E., Matthews K., Aaronson M.,

- 1978, ApJ, 220, 75
- Fulbright J. P., McWilliam A., Rich R. M., 2007, ApJ, 661, 1152
- González J. J., 1993, PhD thesis, University of California, Santa Cruz
- Graves G. J., Schiavon R. P., 2008, ApJS, 177, 446
- Grillo C., Gobat R., Lombardi M., Rosati P., 2009, A&A, 501, 461
- Hardy E., Couture J., 1988, ApJ, 325, L29
- Heckman T. M., Armus L., Miley G. K., 1990, ApJS, 74, 833
- Jorgensen U. G., 1994, A&A, 284, 179
- Korn A. J., Maraston C., Thomas D., 2005, A&A, 438, 685
- Kroupa P., 2001, MNRAS, 322, 231
- La Barbera F., Ferreras I., Vazdekis A., de la Rosa I. G., de Carvalho R. R., Trevisan M., Falcón-Barroso J., Ricciardelli E., 2013, ArXiv e-prints
- Lehnert M. D., Tasse C., Nesvadba N. P. H., Best P. N., van Driel W., 2011, A&A, 532, L3
- Leitherer C. et al., 1999, ApJS, 123, 3
- Lyubenova M., Kuntschner H., Rejkuba M., Silva D. R., Kissler-Patig M., Tacconi-Garman L. E., 2012, A&A, 543, A75
- Maraston C., 2005, MNRAS, 362, 799
- Marigo P., Girardi L., Bressan A., Groenewegen M. A. T., Silva L., Granato G. L., 2008, A&A, 482, 883
- Mould J. R., 1976, A&A, 48, 443
- Napolitano N. R., Romanowsky A. J., Tortora C., 2010, MNRAS, 405, 2351
- Öhman Y., 1934, ApJ, 80, 171
- Peletier R. F., 1989, PhD thesis, University of Groningen, The Netherlands, (1989)
- Peterson R. C., 1976, ApJ, 210, L123
- Pietrinferni A., Cassisi S., Salaris M., Castelli F., 2006, ApJ, 642, 797
- Reimers D., 1975, Memoires of the Societe Royale des Sciences de Liege, 8, 369
- Renzini A., 2006, ARA&A, 44, 141
- Salaris M., Chieffi A., Straniero O., 1993, ApJ, 414, 580
- Salpeter E. E., 1955, ApJ, 121, 161
- Sánchez-Blázquez P. et al., 2006, MNRAS, 371, 703
- Schiavon R. P., 2007, ApJS, 171, 146
- Schiavon R. P., Barbuy B., Bruzual A. G., 2000, ApJ, 532, 453
- Schiavon R. P., Barbuy B., Rossi S. C. F., Milone A., 1997, ApJ, 479, 902
- Schiavon R. P., Barbuy B., Singh P. D., 1997, ApJ, 484, 499
- Serven J., Worthey G., Briley M. M., 2005, ApJ, 627, 754
- Smith R. J., Lucey J. R., 2013, ArXiv e-prints
- Smith R. J., Lucey J. R., Carter D., 2012, MNRAS, 421, 2982
- Smith R. J., Lucey J. R., Hudson M. J., Bridges T. J., 2009, MNRAS, 398, 119
- Spiniello C., Koopmans L. V. E., Trager S. C., Czoske O., Treu T., 2011, MNRAS, 417, 3000
- Spiniello C., Trager S. C., Koopmans L. V. E., Chen Y. P., 2012, ApJ, 753, L32
- Spinrad H., 1962, ApJ, 135, 715
- Spinrad H., Taylor B. J., 1971, ApJS, 22, 445
- Stevenson C. C., 1994, MNRAS, 267, 904
- Thomas D., Maraston C., Bender R., Mendes de Oliveira C., 2005, ApJ, 621, 673
- Thomas J. et al., 2011, MNRAS, 415, 545
- Tortora C., Romanowsky A. J., Napolitano N. R., 2013, ApJ, 765, 8
- Trager S. C., Faber S. M., Dressler A., 2008, MNRAS, 386, 715
- Trager S. C., Faber S. M., Worthey G., González J. J., 2000a, AJ, 120, 165
- , 2000b, AJ, 119, 1645
- Trager S. C., Worthey G., Faber S. M., Burstein D., Gonzalez J. J., 1998, ApJS, 116, 1
- Tremonti C. A. et al., 2004, ApJ, 613, 898
- Treu T., Auger M. W., Koopmans L. V. E., Gavazzi R., Marshall P. J., Bolton A. S., 2010, ApJ, 709, 1195
- Valdes F., Gupta R., Rose J. A., Singh H. P., Bell D. J., 2004, ApJS, 152, 251
- Valenti E., Ferraro F. R., Origlia L., 2010, MNRAS, 402, 1729
- van Dokkum P. G., 2008, ApJ, 674, 29
- van Dokkum P. G., Conroy C., 2010, Nature, 468, 940
- Vazdekis A., Casuso E., Peletier R. F., Beckman J. E., 1996, ApJS, 106, 307
- Vazdekis A., Cenarro A. J., Gorgas J., Cardiel N., Peletier R. F., 2003a, MNRAS, 340, 1317
- Vazdekis A., González J. J., Olguín L., Gorgas J., Cenarro J., Cardiel N., Sánchez-Blázquez P., Pedraz S., 2003b, in Revista Mexicana de Astronomía y Astrofísica Conference Series, Vol. 16, Revista Mexicana de Astronomía y Astrofísica Conference Series, Rodriguez Espinoza J. M., Garzon Lopez F., Melo Martin V., eds., pp. 103–107
- Vazdekis A., Peletier R. F., Beckman J. E., Casuso E., 1997, ApJS, 111, 203
- Vazdekis A., Ricciardelli E., Cenarro A. J., Rivero-González J. G., Díaz-García L. A., Falcón-Barroso J., 2012, MNRAS, 424, 157
- Vazdekis A., Sánchez-Blázquez P., Falcón-Barroso J., Cenarro A. J., Beasley M. A., Cardiel N., Gorgas J., Peletier R. F., 2010, MNRAS, 404, 1639
- White S. D. M., Rees M. J., 1978, MNRAS, 183, 341
- Worthey G., 1992, in IAU Symposium, Vol. 149, The Stellar Populations of Galaxies, Barbuy B., Renzini A., eds., p. 507
- , 1994, ApJS, 95, 107
- , 1998, PASP, 110, 888
- Zaritsky D., Gonzalez A. H., Zabludoff A. I., 2006, ApJ, 638, 725